

Figure 4.63. SEM photomicrographs of failure surfaces for a non-treated lap specimen.

Table 4.26. XPS results (atomic %) for non-treated lap specimens. Two different failure surfaces of the same lap specimen analyzed; arbitrarily labeled side A and side B. Standard deviations are reported at the 95% confidence limit.

Element	Cohesive failure (within the adhesive)	
	Side A	Side B
C	72.9 ± 1.2	73.4 ± 0.5
O	18.4 ± 1.2	18.0 ± 0.5
N	4.9 ± 0.1	5.1 ± 0.2
Si	3.6 ± 0.2	3.2 ± 0.3
Ti	< 0.2	< 0.2
Al	< 0.3	< 0.3
F	< 0.2	< 0.2

nitrogen, and silicon (glass scrim cloth) are typical of the values anticipated for failure surfaces that are produced via debonding within the scrim cloth supported FM-5 adhesive. Also, the shape of carbon 1s photopeak is indicative of polyimide adhesive. The elements titanium, aluminum, and fluorine were either not detected or were present in very small amounts ( $\leq 0.3$  atomic %).

#### *4.4.2 Thermally Treated Lap Specimens*

##### *4.4.2.1 Lap Specimens Thermally Treated at 177°C and 204°C (Bond and Heat)*

The average lap-shear strengths and failure modes (detected by visual inspection) for specimens that were thermally treated at 177°C and 204°C for various times are summarized in Table 4.27. The lap shear specimens that were thermally treated at 177°C for 4 weeks and at 204°C for 1 week exhibited the same failure strength as that for the non-thermally treated specimens. The lap-shear strength decreased to about 44.6 MPa and 44.9 MPa for specimens that had been thermally treated at 177°C for 4 months and at 204°C for 4 weeks, respectively. Visual examination of the failure surfaces for thermally treated (177°C and 204°C) specimens revealed that the debonding occurred primarily in the adhesive (cohesive failure). The visual observations were confirmed by XPS and SEM analysis of the failure surfaces. The SEM photomicrographs of failure surfaces for lap specimens thermally treated at 177°C in air for 4-weeks and 4-months, respectively, are shown in Figure 4.64. Figure 4.65 shows the SEM photomicrographs of failure surfaces for lap specimens thermally treated at 204°C in air for 1-week and 4-weeks, respectively. The weave-type features are evident in the SEM photomicrographs of the failure surfaces which are characteristic of the pattern of the woven glass scrim cloth in the adhesive.

The XPS results for lap specimens thermally treated at 177°C for 4 weeks and 4 months and at 204°C for 1 week and 4 weeks, respectively, are summarized in Tables 4.28 and 4.29. The XPS results confirm that the failure is in the adhesive at the scrim cloth-adhesive interface. The XPS results for the two failure surfaces (Side A and Side B) are equivalent. The atomic

Table 4.27. The lap-shear strengths and failure modes (visual) for specimens thermally treated in air at 177°C and 204°C for various times. Standard deviations are reported at the 95% confidence limit.

Treatment conditions	Lap-shear strength (MPa)	Failure mode (%)	
		cohesive failure (within the adhesive)	adhesive failure (interfacial)
No treatment	49.5 ± 1.5	100	0
177°C/4-weeks	48.8 ± 1.5	100	0
177°C/4-months	44.6 ± 1.8	99	1
204°C/1-week	50.2 ± 1.2	100	0
204°C/4-weeks	44.9 ± 0.7	96	4

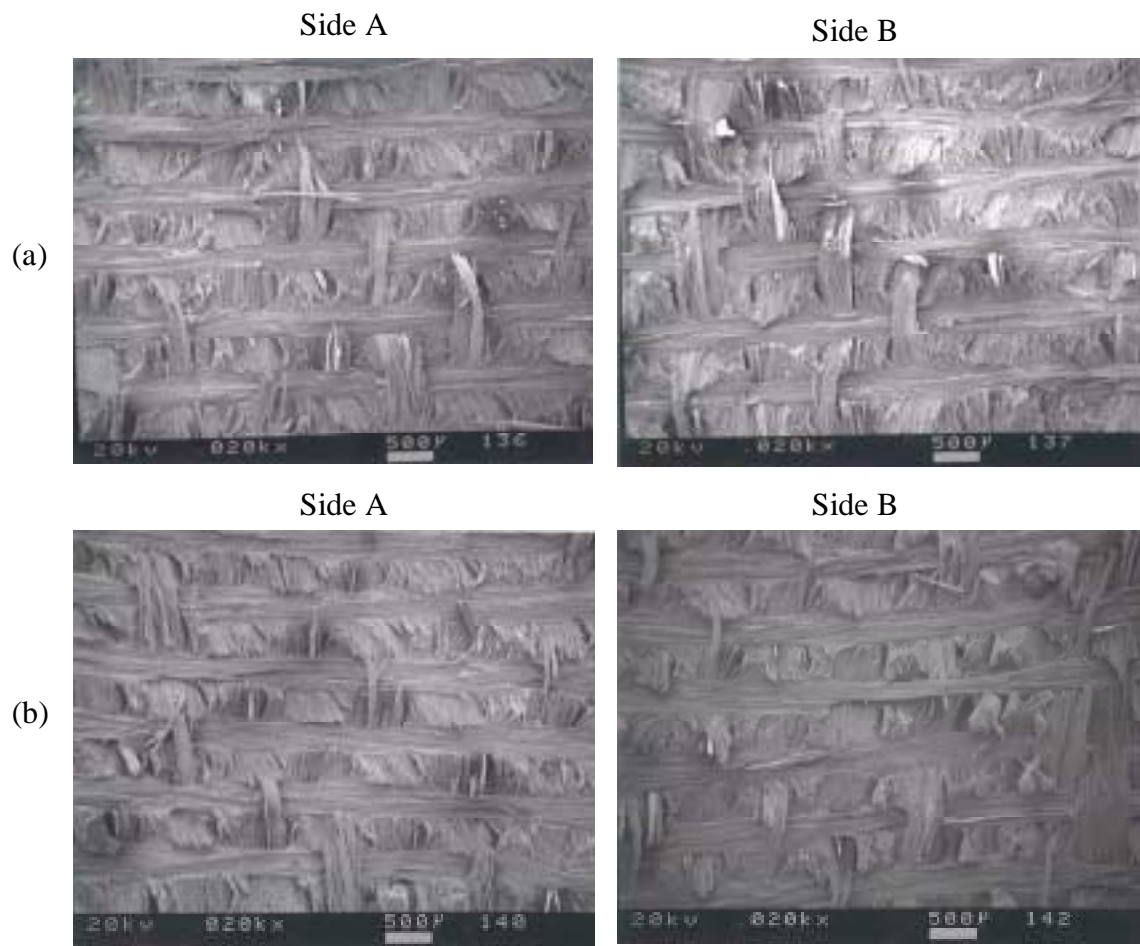


Figure 4.64. SEM photomicrographs of failure surfaces for lap specimens thermally treated at 177°C in air for (a) 4 weeks and (b) 4 months.

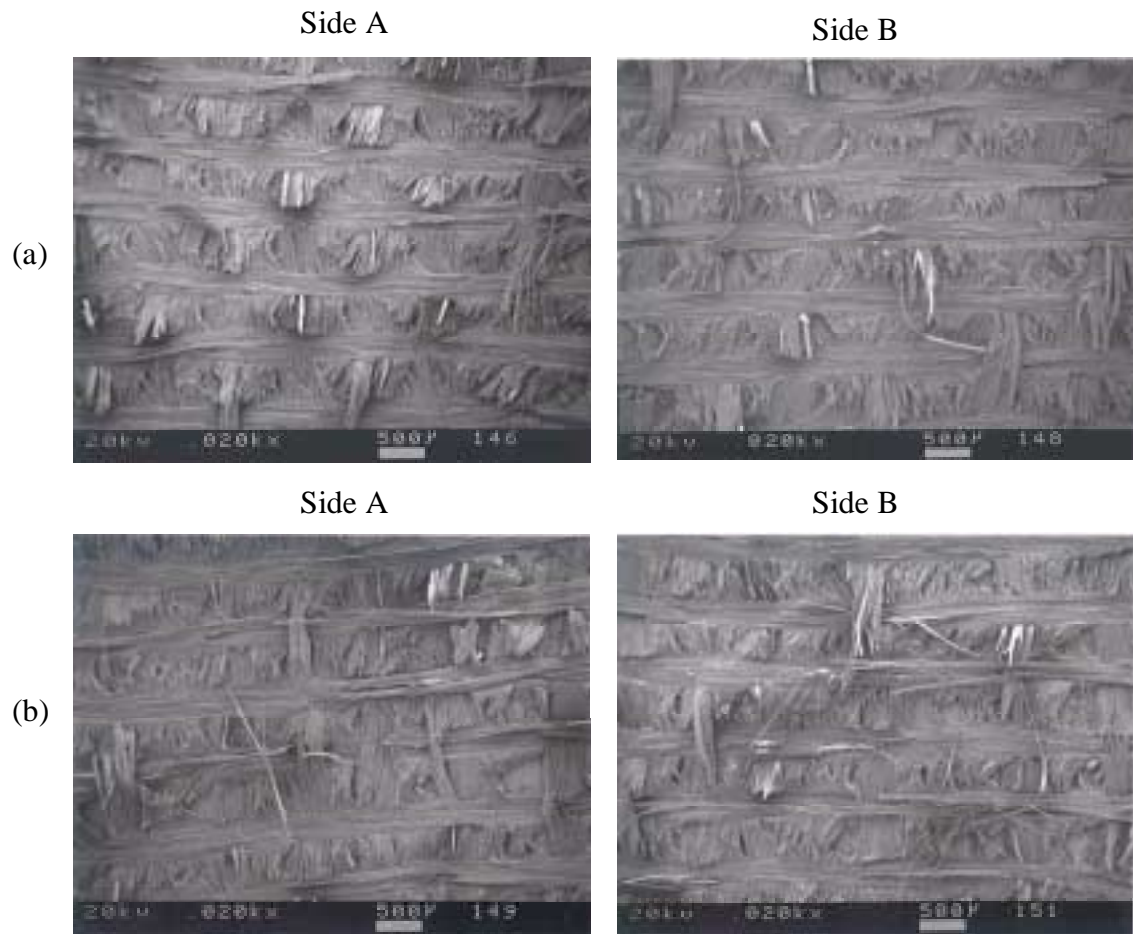


Figure 4.65. SEM photomicrographs of failure surfaces for lap specimens thermally treated at 204°C in air for (a) 1 week and (b) 4 weeks.

Table 4.28. XPS results (atomic %) for lap specimens thermally treated at 177°C, in air, for 4 weeks and 4 months. Standard deviations are reported at the 95% confidence limit.

Element	4 weeks		4 months	
	Side A	Side B	Side A	Side B
C	74.5 ± 0.1	73.4 ± 0.8	75 ± 0.3	73.8 ± 0.1
O	17.5 ± 0.3	18.2 ± 0.4	17.9 ± 0.7	18.0 ± 0.7
N	4.8 ± 0.2	4.7 ± 0.3	4.7 ± 0.1	4.9 ± 0.6
Si	2.8 ± 0.3	3.4 ± 0.2	2.2 ± 0.8	2.9 ± 0
Ti	< 0.2	< 0.2	< 0.2	< 0.2
Al	< 0.3	< 0.3	< 0.3	< 0.3
F	< 0.2	< 0.2	< 0.2	< 0.2

Table 4.29. XPS results (atomic %) for lap specimens thermally treated at 204°C, in air, for 1 week and 4 weeks. Standard deviations are reported at the 95% confidence limit.

Element	1 week		4 weeks	
	Side A	Side B	Side A	Side B
C	74.5 ± 0.5	74.3 ± 0.8	72.5 ± 0.3	74.2 ± 1.8
O	17.1 ± 0.3	17.4 ± 0.7	19.1 ± 0.2	17.5 ± 1.2
N	5.1 ± 0.1	4.9 ± 0.4	4.8 ± 0.4	5.1 ± 0.3
Si	2.7 ± 0.2	2.7 ± 0.1	3.4 ± 0.1	2.8 ± 0.3
Ti	< 0.2	< 0.2	< 0.2	< 0.2
Al	< 0.3	< 0.3	< 0.3	< 0.3
F	0.3 ± 0.1	0.4 ± 0.1	< 0.2	< 0.2

concentrations for carbon, oxygen, nitrogen, and silicon (glass scrim cloth) are typical of the values for failure surfaces that are produced via debonding within the adhesive. Also, the shape of carbon 1s photopeak is indicative of polyimide adhesive, for example, see Figure 4.66. The elements titanium, aluminum, and fluorine were either not detected or were present in very small amounts ( $\leq 0.3$  atomic %).

As discussed in the previous section (for wedge-test data), the loss in lap-shear strength for specimens that were thermally treated at 177°C for 4 weeks and at 204°C for 4 weeks is due to chemical degradation (e.g., chain scissions via thermal oxidation) of adhesive.

#### 4.4.2.2 Lap Specimens Thermally Treated at Elevated Temperatures (350°C-399°C)

The average lap-shear strengths and failure modes (visual inspection) for thermally treated (350°C to 399°C) specimens are summarized in Table 4.30. The lap-shear strengths, as well as the extent of cohesive failure (%), decreased with an increase in treatment time at a given temperature or with an increase in treatment temperature at a comparable time. For example, the photographs of both sides of the failed lap joints for a non-treated specimen and for specimens thermally treated at 399°C for 0.5 hour and 3.0 hours are shown in Figure 4.67. For non-treated lap specimen, the failure is 100% cohesive within the adhesive; scrim cloth is clearly visible on both sides of the failed joint. For the lap specimen thermally treated at 399°C for 0.5 hour, the failure is visually determined to be 55 % cohesive within the adhesive. For the lap specimen thermally treated at 399°C for 3.0 hours, the failure is 100% interfacial (failure within the oxide); both surfaces of the failed joint show metal-like smooth features. For lap specimens thermally treated at 350°C, 371°C, 385°C and 399°C two distinct failure regions were noted on the failed specimens. The regions corresponded to adhesive (interfacial – at the oxide/adhesive interface) or cohesive (within the adhesive) failures. XPS analysis revealed that what appeared (visually) to be a interfacial failure was in fact a failure primarily in the oxide (oxide failure). In a failure that is purely cohesive in the adhesive, the two sides are equivalent and can be arbitrarily

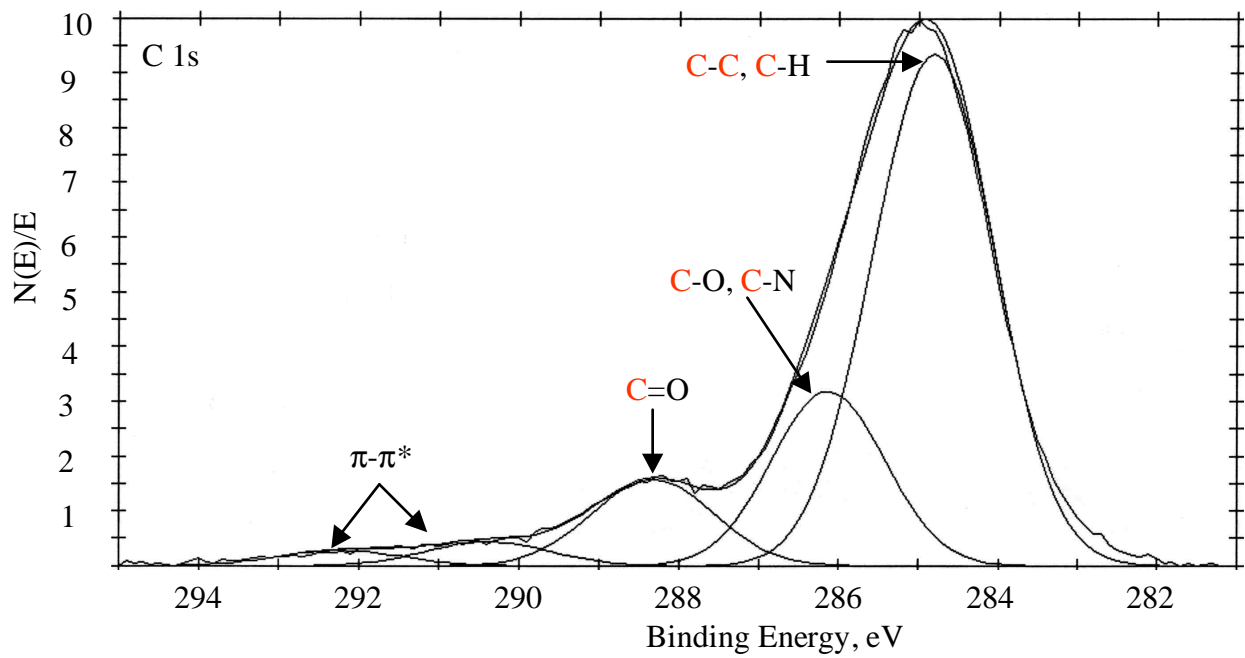


Figure 4.66. The carbon (C 1s) XPS photopeak for Side A failure surface for a lap specimen thermally treated at 204°C for 4 weeks.

Table 4.30. The lap-shear strengths and failure modes (visual) for specimens thermally treated in air at 350°C, 371°C, 385°C and 399°C for various times. Standard deviations are reported at the 95% confidence limit.

Treatment conditions	Lap-shear strength (MPa)	Failure mode (%)	
		cohesive failure (within the adhesive)	adhesive failure (interfacial)
350°C/0.5 hour	39.8 ± 4.7	90	10
350°C/1.0 hour	31.4 ± 1.4	92	8
350°C/2.0 hours	30.2 ± 2.3	91	9
350°C/3.0 hours	35.7 ± 5.8	96	4
350°C/5.0 hours	20.9 ± 1.7	73	27
350°C/11.0 hours	15.2 ± 1.7	59	41
350°C/24.0 hours	9.2 ± 0.5	3	97
371°C/0.5 hour	25.1 ± 1.5	92	8
371°C/1.0 hour	19.7 ± 3.8	68	32
371°C/2.0 hours	14.1 ± 1.1	78	22
371°C/3.0 hours	11.5 ± 2.4	29	71
385°C/0.5 hour	21.7 ± 2.0	82	18
385°C/1.0 hour	9.7 ± 1.0	33	67
385°C/2.0 hours	11.3 ± 2.1	25	75
385°C/3.0 hours	4.1 ± 1.3	3	97
399°C/0.5 hour	11.7 ± 2.2	56	44
399°C/1.0 hour	10.6 ± 1.3	28	72
399°C/2.0 hours	6.2 ± 1.3	1	99
399°C/3.0 hours	3.2 ± 1.2	0	100

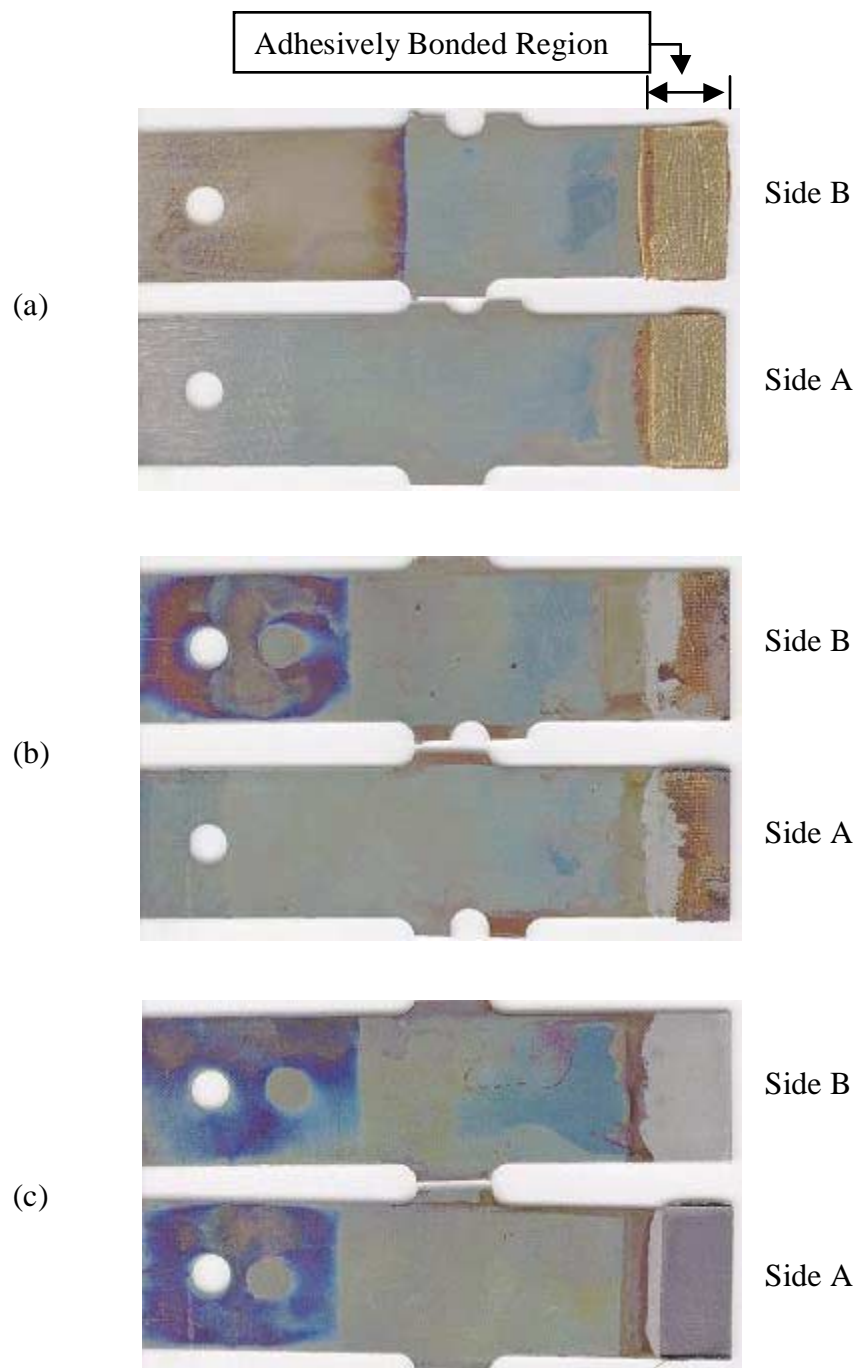


Figure 4.67. The photographs of Side A and Side B failure surfaces for (a) non-treated lap specimen and for specimens that were thermally treated at 399°C for (b) 0.5 hour and 3.0 hours.

assigned Side A and Side B. In a joint failure that exhibits interfacial failure in addition to cohesive failure (both types of failure), the side that has an oxide coating on top of adhesive film in an interfacial failure region is indicated as Side A. The other side that has a very thin coating of oxide on the surface is designated as Side B.

The SEM photomicrographs of the cohesive failure region and interfacial failure region on each failure surface for lap specimens that were thermally treated at 350°C in air for various times, are shown in Figures 4.68 and 4.69, respectively. Each SEM photomicrograph shows the two different sides (Side A and Side B) of the same lap sample; however, the photomicrographs are not necessarily of the corresponding spots on each failure surfaces. The SEM photomicrographs of the cohesive failure region (see Figure 4.68) for specimens thermally treated for 0.5 hour show a weave-type pattern on each failure surfaces. However, as the thermal treatment-time is increased, the lap specimens show progressively less and less of weave-type patterns (the only exception being the specimens thermally treated for 3 hours) on each failure surface. The SEM photomicrographs of the cohesive failure region thus suggest that as the treatment-time is increased the location of failure changes from largely scrim cloth/adhesive interface for specimens thermally treated for 0.5 hour to entirely within the adhesive for specimens thermally treated for greater than or equal to 5 hours. However, lap specimen that was thermally treated at 350°C in air for 3 hours showed a weave-type pattern on each failure surfaces. Recall that for these specimens the lap-shear strength was also significantly higher (contrary to the observed trend) than that for specimens thermally treated for only 1.0 and 2.0 hours, respectively. This discrepancy in data has not been resolved.

For specimens thermally treated at 350°C for various times, the SEM photomicrographs in the interfacial failure region (see Figure 4.69) show increasingly smooth features for both oxide-covered sides A and B. The adhesive film underneath the oxide coating is clearly visible at many places on Side A failure surfaces, and the corresponding oxide covered surface of Side B shows a few adhesive film patches. The bright spots in SEM photomicrographs for the failure surfaces

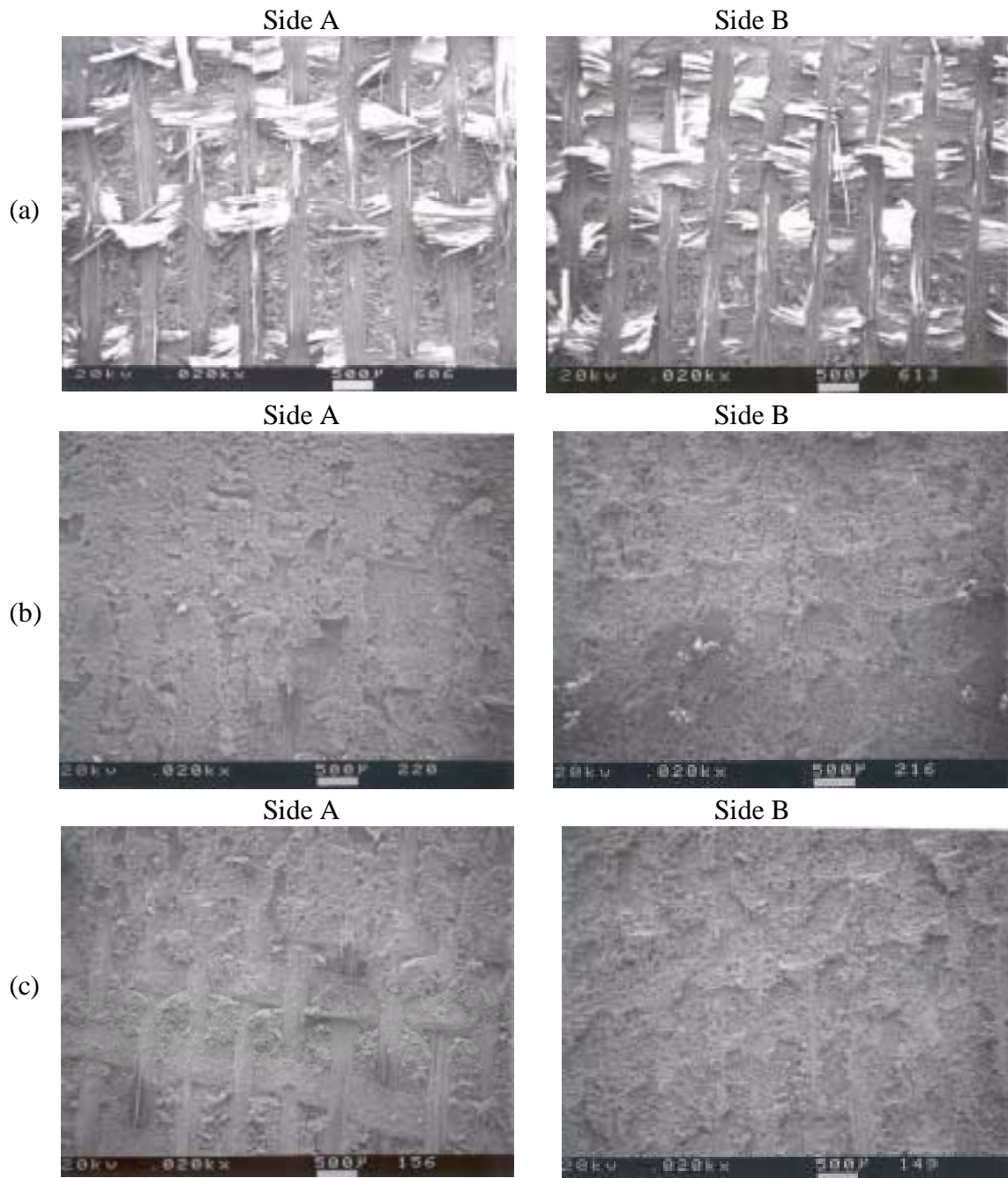


Figure 4.68. The SEM photomicrographs of the cohesive failure regions on each failure surface for lap specimens that were thermally treated at 350°C in air for various times; (a) 0.5 hr, (b) 1.0 hr, and (c) 2.0 hrs.

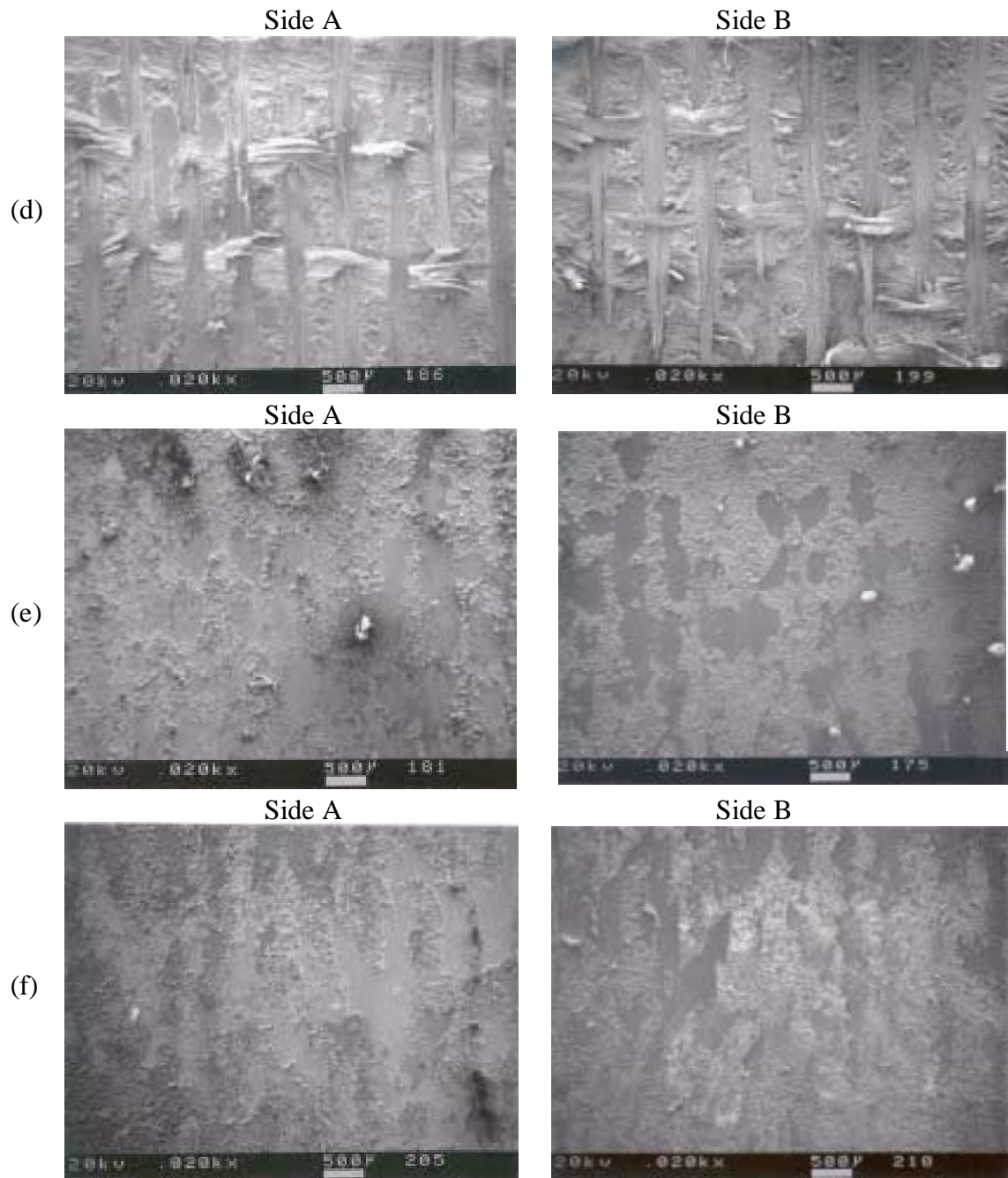


Figure 4.68. (Continued) The SEM photomicrographs of the cohesive failure regions on each failure surface for lap specimens that were thermally treated at 350°C in air for various times; (d) 3.0 hrs, (e) 5.0 hrs, and (f) 11.0 hrs.

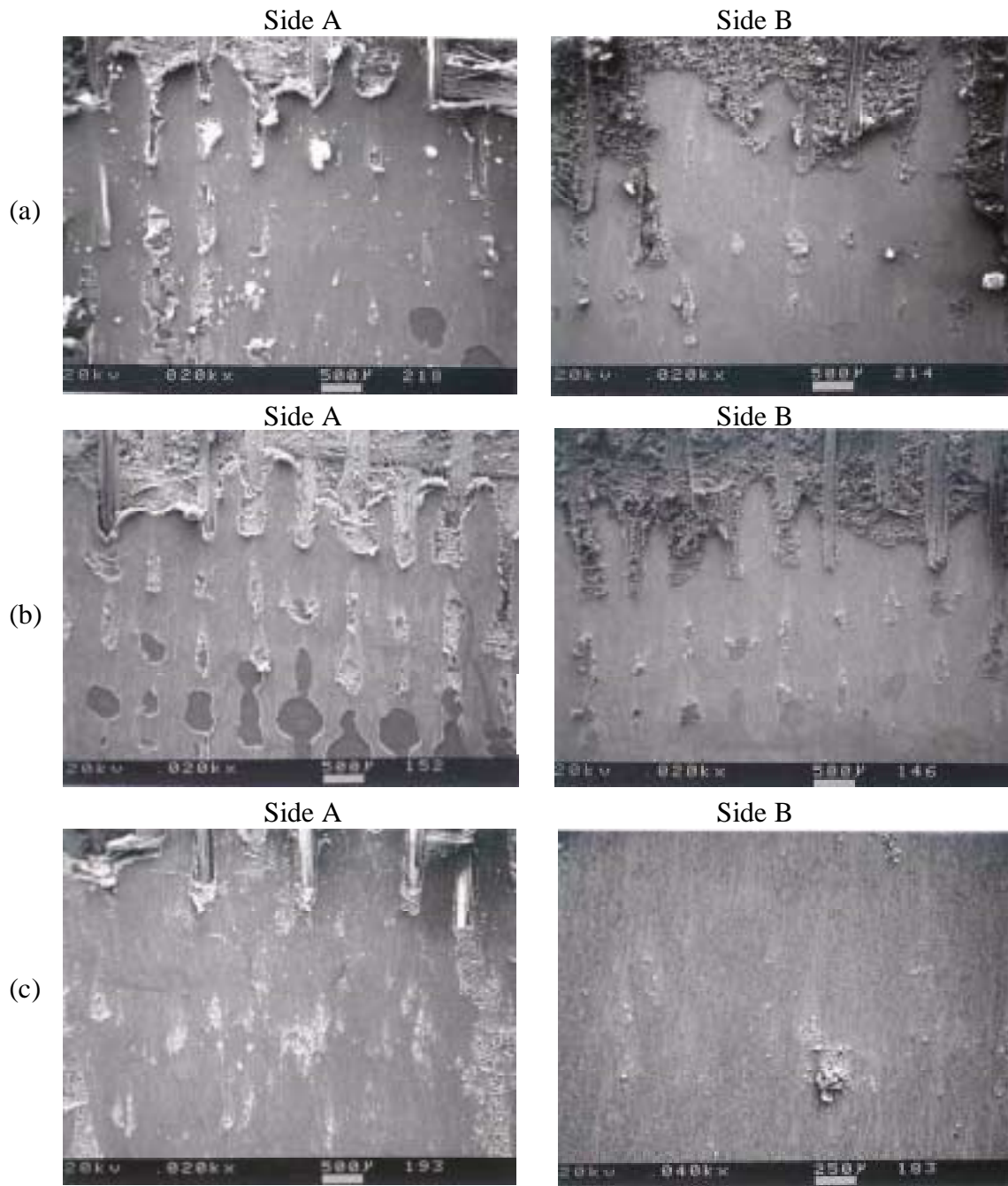


Figure 4.69. The SEM photomicrographs of the oxide failure regions on each failure surface for lap specimens that were thermally treated at 350°C in air for various times; (a) 1.0 hr, (b) 2.0 hrs, and (c) 3.0 hrs.

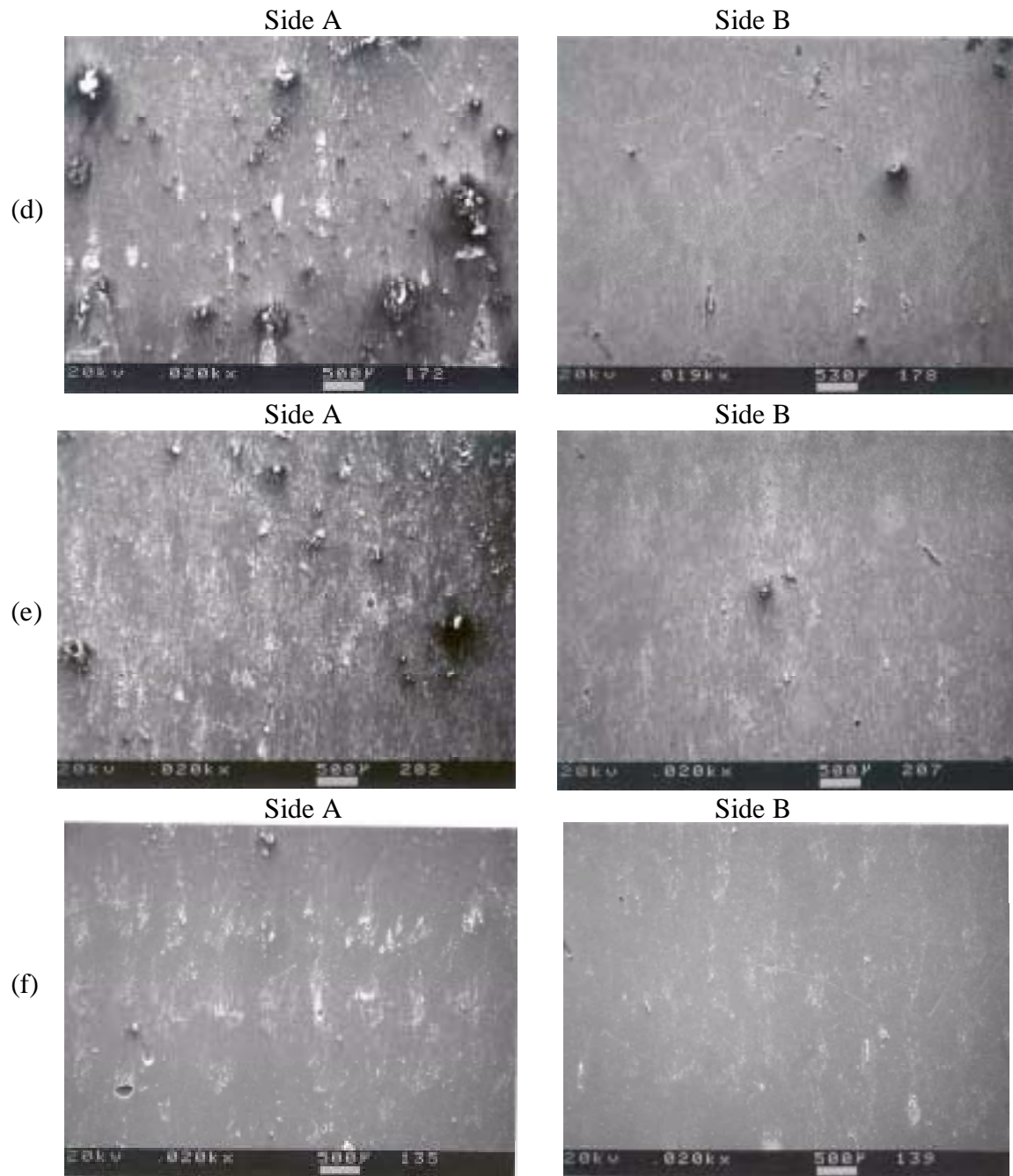


Figure 4.69. (Continued) The SEM photomicrographs of the oxide failure regions on each failure surface for lap specimens that were thermally treated at 350°C in air for various times; (d) 5.0 hrs, (e) 11.0 hrs, and (f) 24 hrs.

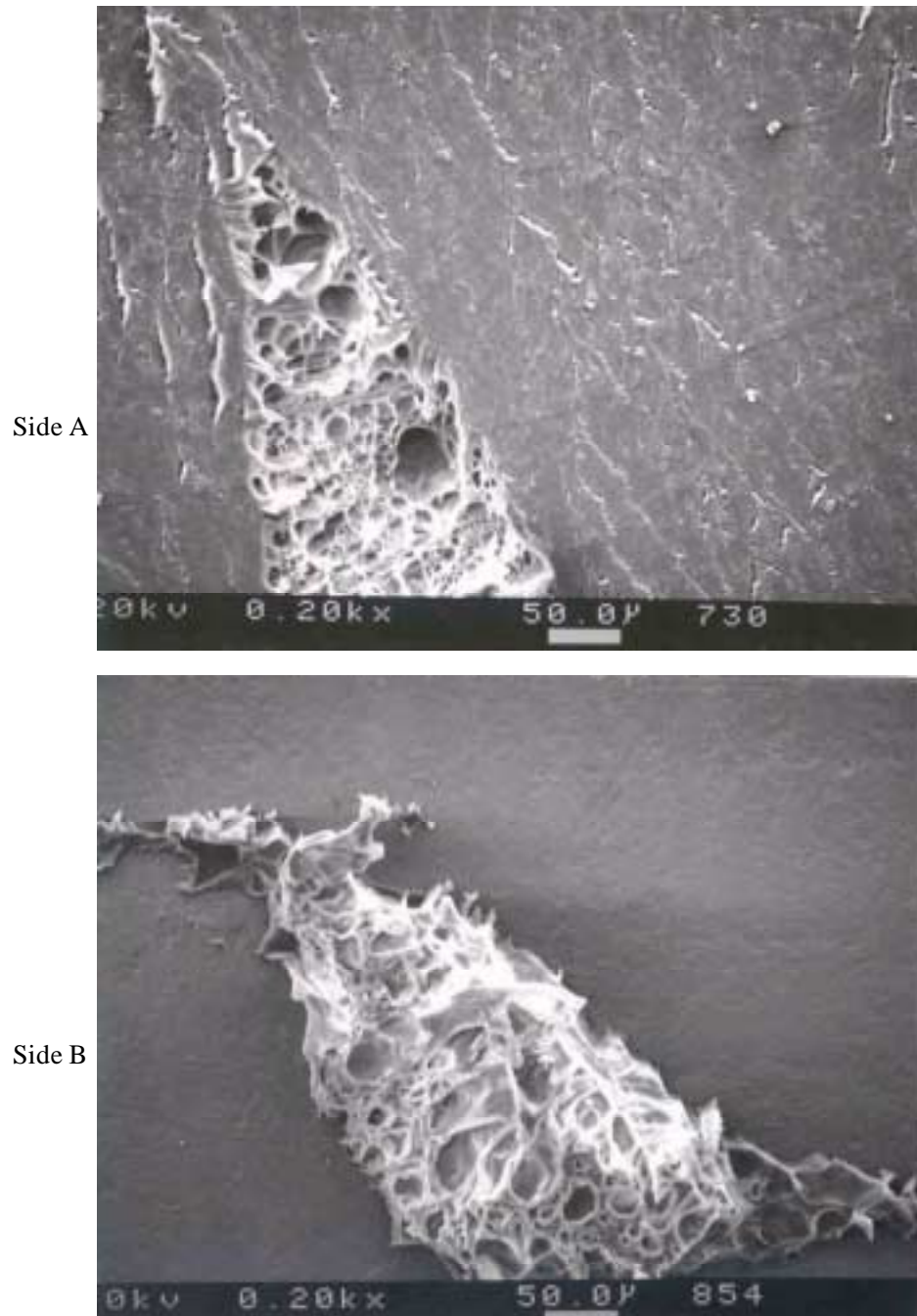


Figure 4.70. The SEM photomicrographs of the interfacial failure region for side A and Side B failure surfaces for a lap specimen that was thermally treated at 371°C for 1.0 hr in air.

represent the exposed adhesives. The SEM photomicrographs in Figure 4.70, obtained at higher magnification, clearly show exposed adhesive film underneath the oxide coating on the Side A failure surface, and an adhesive patch (transferred from Side A) on the corresponding Side B failure surface for a lap specimen thermally treated at 371°C for 3.0 hrs in air. A representative EDX analysis result for the Side A failure surface of a thermally treated (350°C for 5.0 hrs in air) specimen is shown in Figure 4.71. It is apparent from the SEM photomicrographs and the EDX analysis that the oxide failure regions on the failure surfaces contain some small cohesive failure regions as well. This observation is consistent with the XPS results for the oxide failure regions for which small amounts of nitrogen and silicon (indicative of adhesive presence) were found on the failure surfaces. It is also observed that as the treatment-time increased, the extent of cohesive failure in a largely oxide type failure region decreases; this is indicated by a progressive decrease in the number of spots where adhesive is exposed on the Side A and Side B failure surfaces.

The SEM photomicrographs of the oxide failure regions for lap specimens thermally treated in air for 371°C, 385°C and 399°C for 0.5 hrs, 1.0 hr, 2.0 hrs and 3.0 hrs, respectively, are shown in Figures 4.72 – 4.74. The surface features are similar to the features noted in the oxide failure regions for lap specimens thermally treated at 350°C for various times. In general, it is also observed that at a comparable thermal treatment-time, the extent of cohesive failure in a largely oxide type failure region is less for specimens treated at higher temperatures. The SEM photomicrographs of various failure surfaces of thermally treated lap specimens thus suggest that as the thermal treatment-temperature or -time is increased, the oxide failure regions on the failure surfaces increasingly become purely an oxide failure.

XPS analyses of the cohesive failure regions and interfacial failure regions are given in Tables 4.31 – 4.49 for lap shear samples that had been bonded and thermally treated in air at 350°C, 371°C, 385°C and 399°C, respectively, for various times, and tested. Irrespective of the thermal history of the sample, the XPS results for both failure surfaces in the cohesive failure regions were equivalent. These “cohesive” failure surfaces contain carbon, oxygen, nitrogen, and silicon

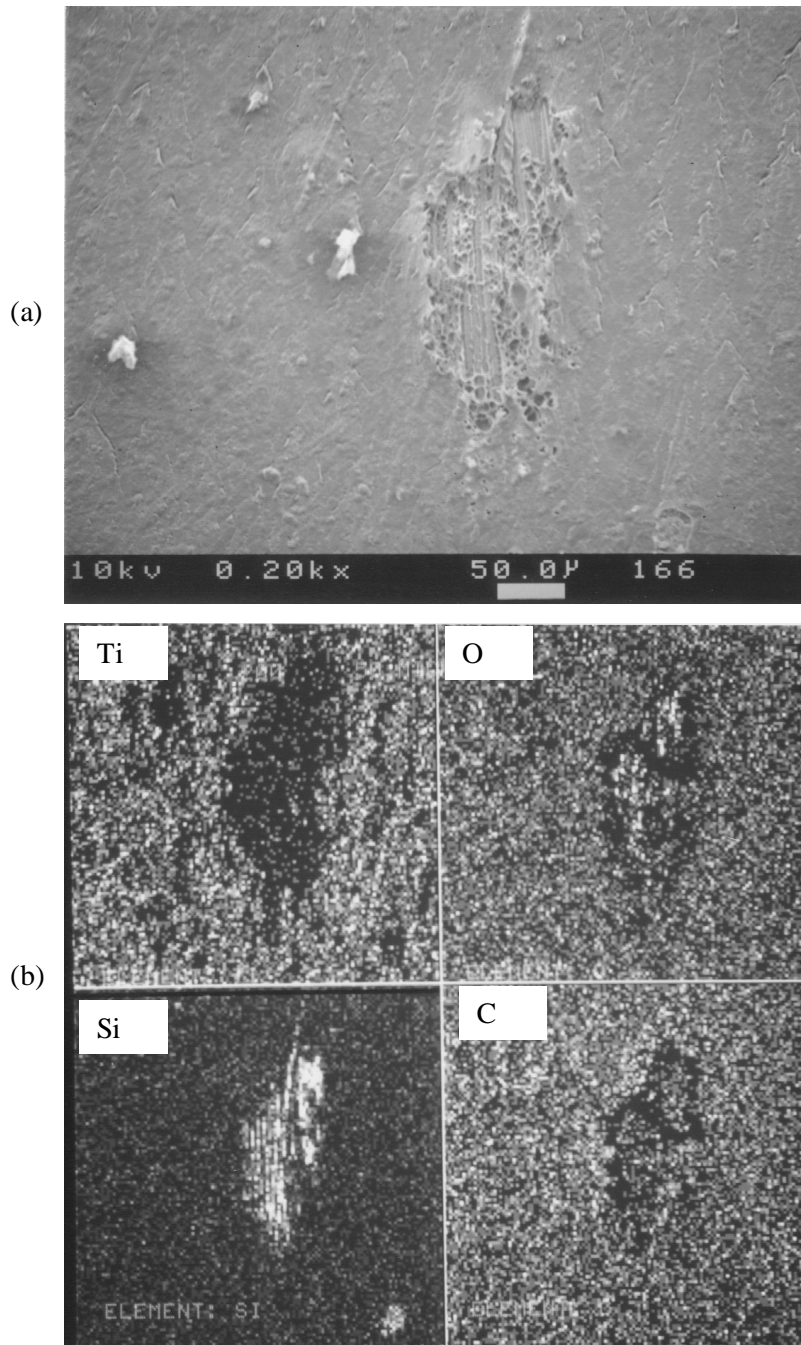


Figure 4.71. SEM photomicrograph and EDX analysis of interfacial failure region for Side A failure surface for a lap specimen thermally treated at 350°C for 5.0 hrs in air; (a) SEM photomicrograph and (b) EDX analysis results for titanium (Ti), oxygen (O), silicon (Si) and carbon (C).

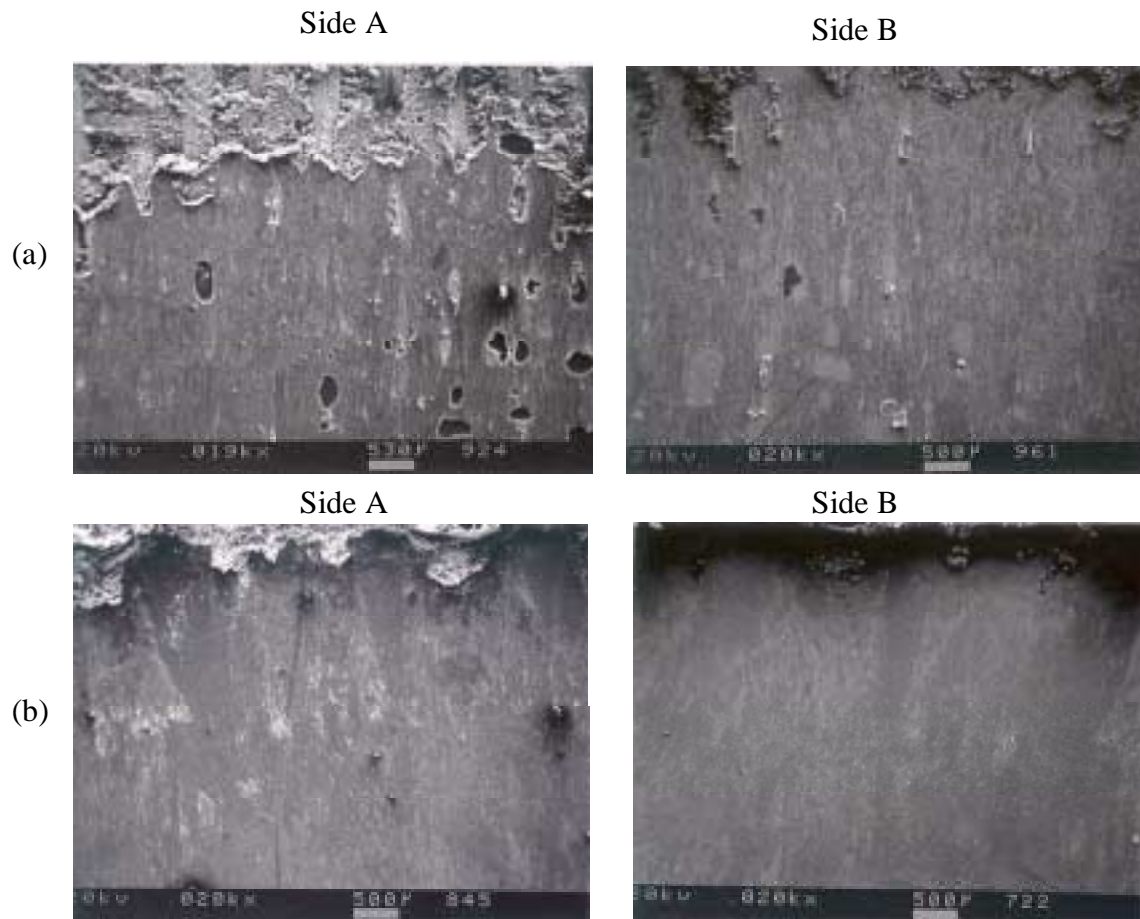


Figure 4.72. The SEM photomicrographs of the oxide failure regions on each failure surface for lap specimens that were thermally treated at 371°C in air for various times; (a) 0.5 hr and (b) 1.0 hr.

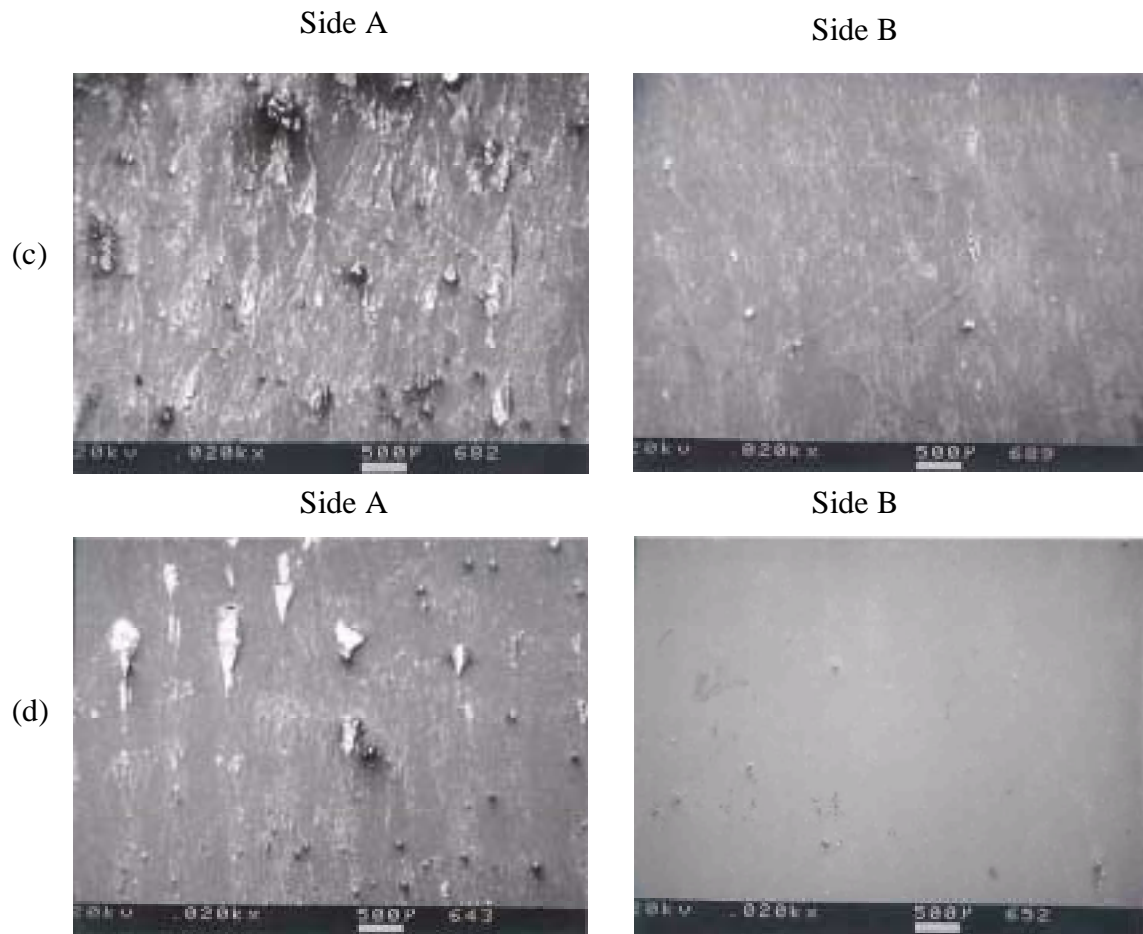


Figure 4.72. (Continued) The SEM photomicrographs of the oxide failure regions on each failure surface for lap specimens that were thermally treated at 371°C in air for various times; (c) 2.0 hrs and (d) 3.0 hrs.

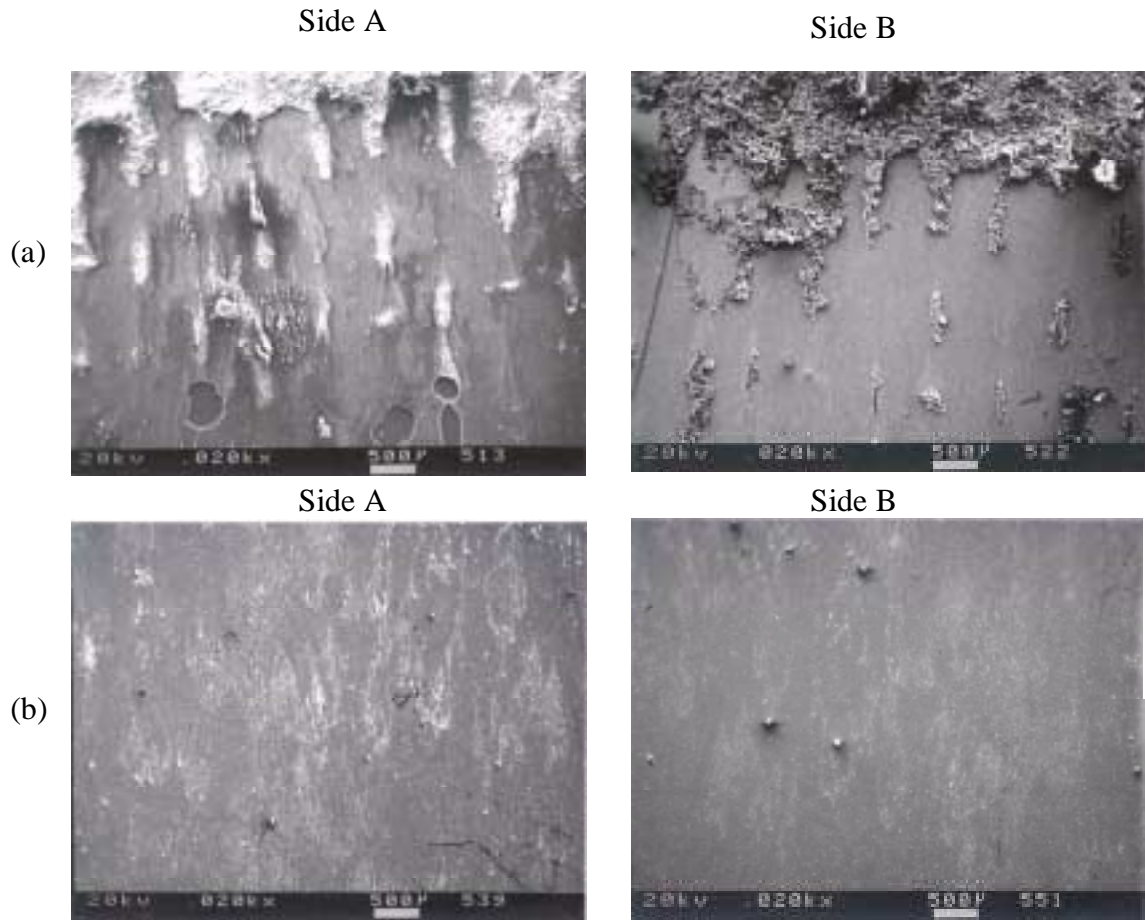


Figure 4.73. The SEM photomicrographs of the oxide failure regions on each failure surface for lap specimens that were thermally treated at 385°C in air for various times; (a) 0.5 hr and (b) 1.0 hr.

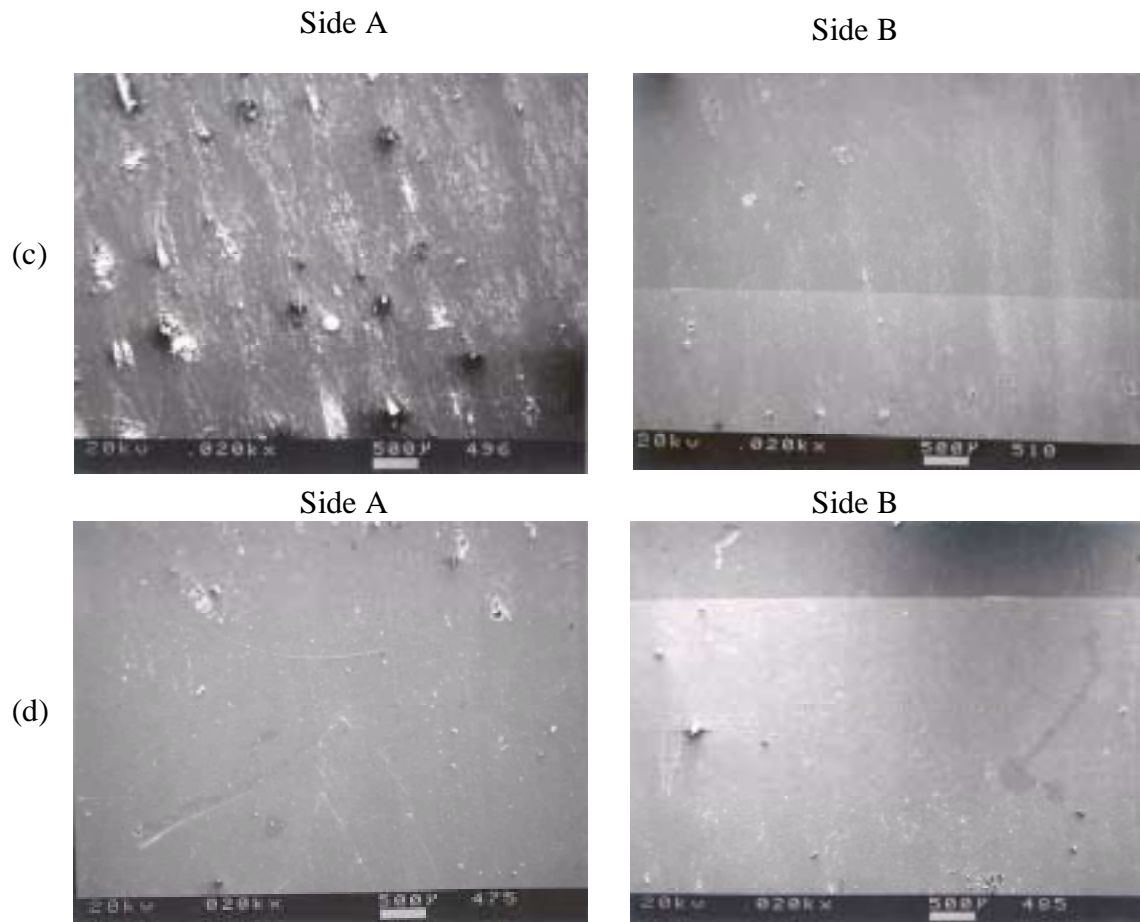


Figure 4.73. (Continued) The SEM photomicrographs of the oxide failure regions on each failure surface for lap specimens that were thermally treated at 385°C in air for various times; (c) 2.0 hrs and (d) 3.0 hrs.

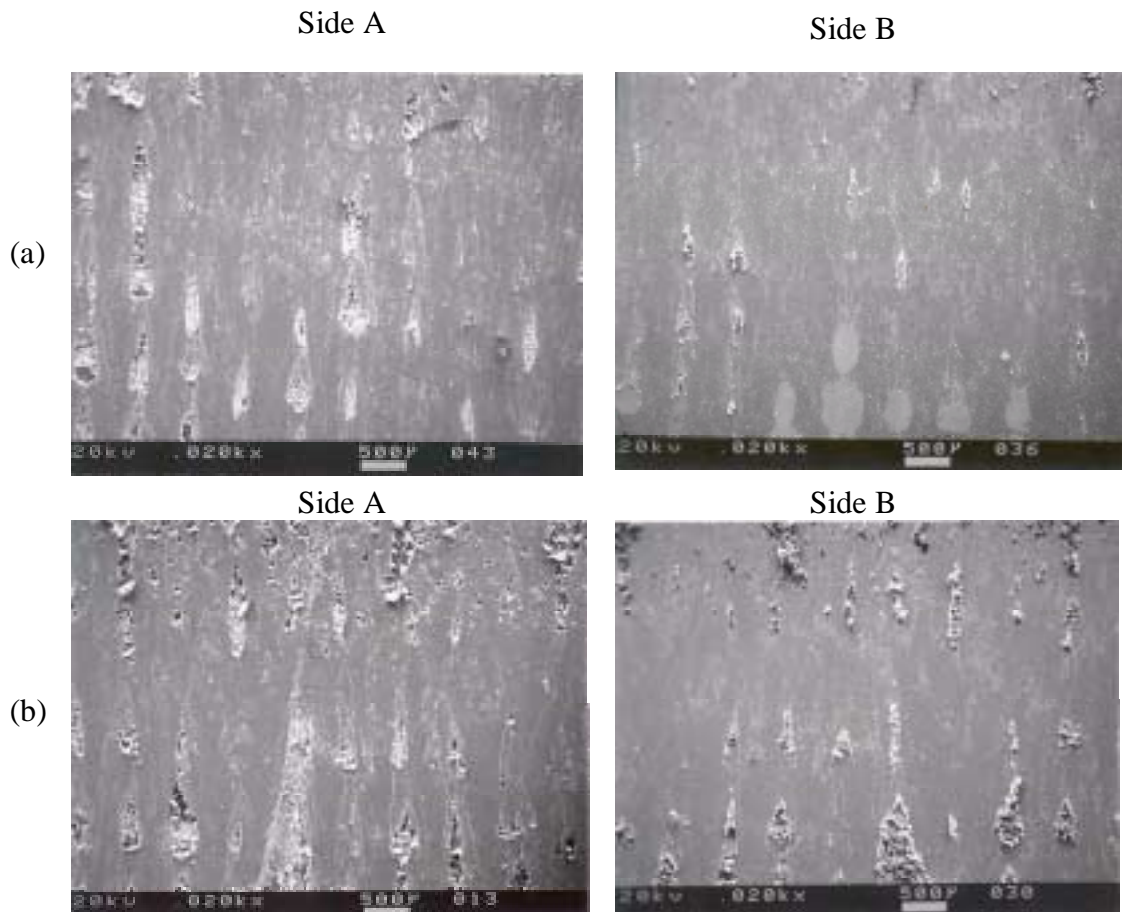


Figure 4.74. The SEM photomicrographs of the oxide failure regions on each failure surface for lap specimens that were thermally treated at 399°C in air for various times; (a) 0.5 hr and (b) 1.0 hr.

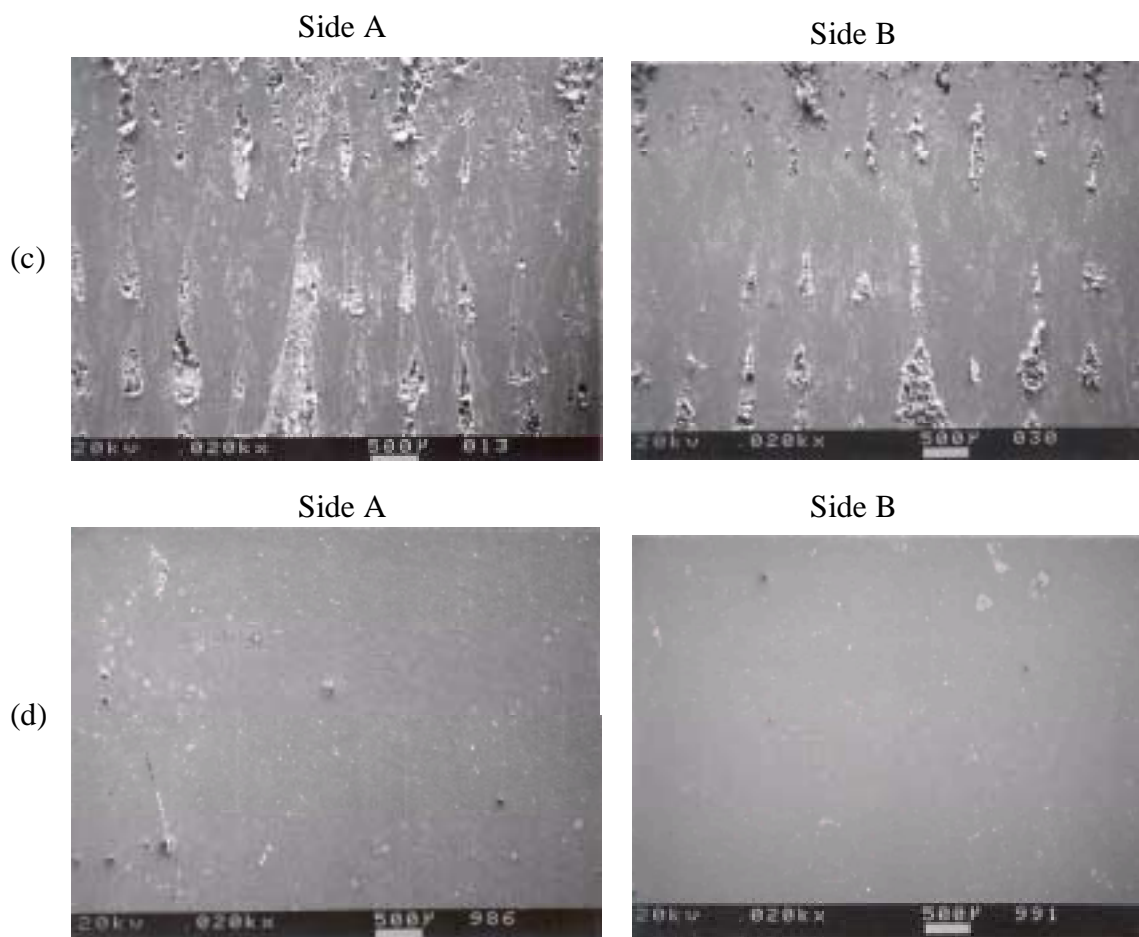


Figure 4.74. (Continued) The SEM photomicrographs of the oxide failure regions on each failure surface for lap specimens that were thermally treated at 399°C in air for various times; (c) 2.0 hrs and (d) 3.0 hrs.

Table 4.31. XPS results (atomic %) for both failure surfaces in the cohesive failure region for lap specimens thermally treated at 350°C for 0.5 hour, in air. Standard deviations are reported at the 95% confidence limit.

Element	Cohesive failure (within the adhesive)	
	Side A	Side B
C	77.0 ± 1.0	75.0 ± 1.5
O	15.7 ± 0.6	17.0 ± 0.9
N	4.7 ± 0.4	4.6 ± 0.1
Si	2.1 ± 0.5	3.1 ± 0.6
Ti	< 0.2	< 0.2
Al	< 0.3	< 0.3
F	0.4 ± 0.3	< 0.2

Table 4.32. XPS results (atomic %) for both failure surfaces in the cohesive failure region and interfacial failure region for lap specimens thermally treated at 350°C for 1.0 hour, in air. Standard deviations are reported at the 95% confidence limit.

Element	Cohesive failure (within the adhesive)		Adhesive failure (interfacial)	
	Side A	Side B	Side A	Side B
C	78.0 ± 0.4	78.1 ± 0.6	57.4 ± 1.4	52.7 ± 1.5
O	14.9 ± 0.3	14.9 ± 0.4	25.3 ± 0.7	30.8 ± 1.2
N	5.0 ± 0.3	5.0 ± 0.3	3.7 ± 0.3	1.4 ± 0.1
Si	2.0 ± 0.1	1.8 ± 0.2	1.7 ± 0.2	7.6 ± 0.4
Ti	< 0.2	< 0.2	5.9 ± 0.2	5.5 ± 0.8
Al	< 0.3	< 0.3	1.9 ± 0.1	1.4 ± 0.2
F	< 0.2	< 0.2	4.2 ± 0.3	0.6 ± 0.4

Table 4.33. XPS results (atomic %) for both failure surfaces in the cohesive failure region and interfacial failure region for lap specimens thermally treated at 350°C for 2.0 hours, in air. Standard deviations are reported at the 95% confidence limit.

Element	Cohesive failure (within the adhesive)		Adhesive failure (interfacial)	
	Side A	Side B	Side A	Side B
C	77.9 ± 0.9	77.7 ± 0.2	56.9 ± 2.8	60.1 ± 0.9
O	14.9 ± 0.8	15.6 ± 0.2	25.0 ± 2.3	26.2 ± 1.0
N	4.1 ± 0.5	4.7 ± 0.2	3.2 ± 0.7	2.5 ± 0.6
Si	2.6 ± 0.1	1.8 ± 0.4	1.5 ± 0.4	2.7 ± 0.3
Ti	< 0.2	< 0.2	6.2 ± 0.8	5.8 ± 0.2
Al	< 0.3	< 0.3	1.8 ± 0.2	1.3 ± 0.1
F	< 0.2	< 0.2	5.3 ± 0.6	1.3 ± 0.2

Table 4.34. XPS results (atomic %) for both failure surfaces in the cohesive failure region and interfacial failure region for lap specimens thermally treated at 350°C for 3.0 hours, in air. Standard deviations are reported at the 95% confidence limit.

Element	Cohesive failure (within the adhesive)		Adhesive failure (interfacial)	
	Side A	Side B	Side A	Side B
C	75.9 ± 0.4	75.5 ± 1.3	53.5 ± 5.0	51.8 ± 4.7
O	16.9 ± 0.7	16.8 ± 0.9	28.3 ± 2.4	33.8 ± 2.9
N	4.5 ± 0.2	5.0 ± 0.3	3.0 ± 0.1	2.6 ± 0.7
Si	2.5 ± 0.3	2.4 ± 0.2	1.5 ± 0.7	2.3 ± 0.8
Ti	< 0.2	< 0.2	6.9 ± 1.3	7.4 ± 1.4
Al	< 0.3	< 0.3	1.7 ± 0.4	1.4 ± 0.6
F	< 0.2	< 0.2	5.0 ± 1.0	0.8 ± 0.6

Table 4.35. XPS results (atomic %) for both failure surfaces in the cohesive failure region and interfacial failure region for lap specimens thermally treated at 350°C for 5.0 hours, in air. Standard deviations are reported at the 95% confidence limit.

Element	Cohesive failure (within the adhesive)		Adhesive failure (interfacial)	
	Side A	Side B	Side A	Side B
C	74.3 ± 1.1	75.0 ± 2.1	48.7 ± 2.7	42.5 ± 2.3
O	17.8 ± 1.0	17.2 ± 0.9	30.6 ± 1.1	39.2 ± 2.0
N	3.9 ± 0.5	4.3 ± 0.4	2.4 ± 0.4	2.2 ± 0.1
Si	3.6 ± 0.5	3.2 ± 0.8	1.2 ± 0.2	2.5 ± 0.6
Ti	< 0.2	< 0.2	9.0 ± 0.4	9.8 ± 0.6
Al	< 0.3	< 0.3	2.4 ± 0.2	2.2 ± 0.2
F	< 0.2	< 0.2	5.7 ± 0.7	1.7 ± 0.1

Table 4.36. XPS results (atomic %) for both failure surfaces in the cohesive failure region and interfacial failure region for lap specimens thermally treated at 350°C for 11.0 hours, in air. Standard deviations are reported at the 95% confidence limit.

Element	Cohesive failure (within the adhesive)		Adhesive failure (interfacial)	
	Side A	Side B	Side A	Side B
C	72.3 ± 1.8	66.5 ± 0.1	42.6 ± 3.1	37.7 ± 1.8
O	19.1 ± 1.8	22.7 ± 0.2	34.4 ± 1.5	43.0 ± 2.0
N	3.8 ± 1.6	3.3 ± 0.6	2.2 ± 0.3	1.8 ± 0.3
Si	4.4 ± 1.8	6.7 ± 1.0	1.2 ± 0.4	1.6 ± 0.8
Ti	< 0.2	0.5 ± 0.5	9.7 ± 1.0	11.8 ± 1.0
Al	< 0.3	< 0.3	3.2 ± 0.3	2.3 ± 0.6
F	0.3 ± 0.1	< 0.2	6.8 ± 0.7	1.7 ± 0.1

Table 4.37. XPS results (atomic %) for both failure surfaces in the interfacial failure region for lap specimens thermally treated at 350°C for 24.0 hours, in air. Standard deviations are reported at the 95% confidence limit.

Element	Adhesive failure (interfacial)	
	Side A	Side B
C	24.5 ± 2.9	30.4 ± 8.7
O	38.4 ± 1.1	45.3 ± 5.7
N	1.7 ± 0.2	0.8 ± 0.3
Si	2.3 ± 0.4	3.6 ± 0.2
Ti	13.0 ± 0.2	13.1 ± 1.5
Al	4.4 ± 0.3	2.6 ± 0.8
F	15.7 ± 1.2	4.2 ± 0.5

Table 4.38. XPS results (atomic %) for both failure surfaces in the cohesive failure region and interfacial failure region for lap specimens thermally treated at 371°C for 0.5 hour, in air. Standard deviations are reported at the 95% confidence limit.

Element	Cohesive failure (within the adhesive)		Adhesive failure (interfacial)	
	Side A	Side B	Side A	Side B
C	76.8 ± 0.4	74.9 ± 0.3	46.9 ± 1.9	44.2 ± 4.9
O	15.6 ± 0.3	17.7 ± 0.2	31.5 ± 1.9	38.0 ± 3.5
N	5.1 ± 0.1	4.4 ± 0.2	2.3 ± 0.3	2.0 ± 0.1
Si	2.2 ± 0.1	2.9 ± 0.1	1.5 ± 0.2	2.8 ± 0.5
Ti	< 0.2	< 0.2	9.1 ± 0.6	9.7 ± 1.2
Al	< 0.3	< 0.3	2.5 ± 0.3	1.8 ± 0.3
F	< 0.2	< 0.2	6.2 ± 0.9	1.5 ± 0.4

Table 4.39. XPS results (atomic %) for both failure surfaces in the cohesive failure region and interfacial failure region for lap specimens thermally treated at 371°C for 1.0 hour, in air. Standard deviations are reported at the 95% confidence limit.

Element	Cohesive failure (within the adhesive)		Adhesive failure (interfacial)	
	Side A	Side B	Side A	Side B
C	78.2 ± 0.4	77.8 ± 0.4	38.0 ± 1.0	33.9 ± 2.7
O	15.0 ± 0.6	15.3 ± 0.4	34.4 ± 0.5	44.0 ± 1.9
N	4.7 ± 0.3	4.5 ± 0.5	1.9 ± 0.1	1.6 ± 0.2
Si	1.9 ± 0.1	2.2 ± 0.4	2.3 ± 0.2	4.0 ± 0.2
Ti	< 0.2	< 0.2	10.7 ± 0.4	11.9 ± 0.7
Al	< 0.3	< 0.3	3.3 ± 0.2	2.3 ± 0.1
F	< 0.2	< 0.2	9.4 ± 0.7	2.4 ± 0.1

Table 4.40. XPS results (atomic %) for both failure surfaces in the cohesive failure region and interfacial failure region for lap specimens thermally treated at 371°C for 2.0 hours, in air. Standard deviations are reported at the 95% confidence limit.

Element	Cohesive failure (within the adhesive)		Adhesive failure (interfacial)	
	Side A	Side B	Side A	Side B
C	72.1 ± 1.8	75.2 ± 0.6	35.7 ± 1.5	28.7 ± 1.3
O	19.1 ± 1.2	17.3 ± 0.4	35.1 ± 0.6	47.7 ± 1.4
N	4.2 ± 0.2	4.2 ± 0	2.2 ± 0.3	1.8 ± 0.1
Si	3.3 ± 0.2	2.6 ± 0	2.3 ± 0.4	3.9 ± 0.6
Ti	0.7 ± 0.4	0.3 ± 0.3	11.0 ± 0.6	12.2 ± 0.1
Al	0.3 ± 0.1	< 0.3	3.6 ± 0.1	2.2 ± 0.2
F	0.3 ± 0	0.3 ± 0.3	10.1 ± 1.0	3.4 ± 0.3

Table 4.41. XPS results (atomic %) for both failure surfaces in the cohesive failure region and interfacial failure region for lap specimens thermally treated at 371°C for 3.0 hours, in air. Standard deviations are reported at the 95% confidence limit.

Element	Cohesive failure (within the adhesive)		Adhesive failure (interfacial)	
	Side A	Side B	Side A	Side B
C	71.8 ± 5.2	71.5 ± 4.3	28.4 ± 4.7	27.2 ± 4.4
O	19.8 ± 3.0	19.8 ± 2.6	38.4 ± 0.3	47.7 ± 1.1
N	3.9 ± 0.4	4.2 ± 0.5	1.5 ± 0.2	1.4 ± 0.4
Si	4.1 ± 2.4	4.0 ± 2.1	2.7 ± 0.2	3.8 ± 0.3
Ti	< 0.2	< 0.2	12.5 ± 1.1	13.6 ± 1.2
Al	< 0.3	< 0.3	3.9 ± 0.3	2.7 ± 0.4
F	< 0.2	< 0.2	12.6 ± 3.3	3.6 ± 1.8

Table 4.42. XPS results (atomic %) for both failure surfaces in the cohesive failure region and interfacial failure region for lap specimens thermally treated at 385°C for 0.5 hour, in air. Standard deviations are reported at the 95% confidence limit.

Element	Cohesive failure (within the adhesive)		Adhesive failure (interfacial)	
	Side A	Side B	Side A	Side B
C	77.6 ± 0.2	77.8 ± 0.8	60.8 ± 14.8	46.9 ± 3.0
O	14.9 ± 0.3	15.0 ± 0.1	23.7 ± 7.9	35.6 ± 2.5
N	5.3 ± 0.3	4.7 ± 0.4	3.4 ± 1.1	1.9 ± 0.3
Si	2.1 ± 0.1	2.2 ± 0.5	2.2 ± 0.3	3.7 ± 0.5
Ti	< 0.2	< 0.2	4.7 ± 4.1	8.5 ± 0.6
Al	< 0.3	< 0.3	1.6 ± 1.2	1.6 ± 0.3
F	< 0.2	< 0.2	3.7 ± 3.0	1.9 ± 0.2

Table 4.43. XPS results (atomic %) for both failure surfaces in the cohesive failure region and interfacial failure region for lap specimens thermally treated at 385°C for 1.0 hour, in air. Standard deviations are reported at the 95% confidence limit.

Element	Cohesive failure (within the adhesive)		Adhesive failure (interfacial)	
	Side A	Side B	Side A	Side B
C	70.3 ± 4.1	72.3 ± 1.2	27.9 ± 4.6	20.5 ± 1.6
O	19.3 ± 1.6	18.8 ± 1.0	37.9 ± 2.2	51.3 ± 0.4
N	3.9 ± 0.3	4.1 ± 0.2	1.5 ± 0.3	1.4 ± 0.2
Si	4.2 ± 0.1	3.9 ± 0	3.3 ± 0.4	5.7 ± 0.9
Ti	0.9 ± 0.9	0.6 ± 0	12.1 ± 0.8	13.8 ± 0.5
Al	< 0.3	< 0.3	3.9 ± 0.5	3.0 ± 0.4
F	1.2 ± 1.1	< 0.2	13.4 ± 0.8	4.4 ± 0.4

Table 4.44. XPS results (atomic %) for both failure surfaces in the interfacial failure region for lap specimens thermally treated at 385°C for 2.0 hours, in air. Standard deviations are reported at the 95% confidence limit.

Element	Adhesive failure (interfacial)	
	Side A	Side B
C	23.7 ± 2.7	22.4 ± 1.6
O	39.3 ± 0.5	50.2 ± 1.4
N	1.4 ± 0.6	1.3 ± 0.4
Si	2.5 ± 0.3	4.1 ± 0.3
Ti	13.0 ± 1.0	14.3 ± 0.3
Al	4.8 ± 0.3	3.1 ± 0.2
F	15.3 ± 0.9	4.6 ± 0.4

Table 4.45. XPS results (atomic %) for both failure surfaces in the interfacial failure region for lap specimens thermally treated at 385°C for 3.0 hours, in air. Standard deviations are reported at the 95% confidence limit.

Element	Adhesive failure (interfacial)	
	Side A	Side B
C	18.5 ± 1.7	15.3 ± 2.3
O	39.0 ± 1.6	54.9 ± 0.5
N	1.5 ± 0.2	0.9 ± 0.2
Si	3.9 ± 0.3	5.7 ± 0.3
Ti	12.7 ± 0.1	15.4 ± 0.3
Al	5.1 ± 0.5	2.9 ± 0.4
F	19.3 ± 0.3	5.0 ± 1.0

Table 4.46. XPS results (atomic %) for both failure surfaces in the cohesive failure region and interfacial failure region for lap specimens thermally treated at 399°C for 0.5 hour, in air. Standard deviations are reported at the 95% confidence limit.

Element	Cohesive failure (within the adhesive)		Adhesive failure (interfacial)	
	Side A	Side B	Side A	Side B
C	75.8 ± 0.8	75.0 ± 0.6	35.0 ± 1.8	29.9 ± 2.5
O	16.4 ± 0.9	16.9 ± 0.4	36.9 ± 2.3	47.1 ± 0.9
N	4.5 ± 0.4	4.4 ± 0.3	1.8 ± 0.3	1.4 ± 0.1
Si	3.0 ± 0.5	3.5 ± 0.9	2.5 ± 0.2	4.5 ± 0.2
Ti	< 0.2	< 0.2	11.2 ± 0.6	12.3 ± 1.6
Al	< 0.3	< 0.3	3.6 ± 0.3	2.5 ± 0.2
F	< 0.2	< 0.2	9.0 ± 1.3	2.3 ± 0.7

Table 4.47. XPS results (atomic %) for both failure surfaces in the cohesive failure region and interfacial failure region for lap specimens thermally treated at 399°C for 1.0 hour, in air. Standard deviations are reported at the 95% confidence limit.

Element	Cohesive failure (within the adhesive)		Adhesive failure (interfacial)	
	Side A	Side B	Side A	Side B
C	73.8 ± 0.4	74.3 ± 0.4	34.5 ± 1.5	30.9 ± 2.0
O	17.5 ± 0.4	17.7 ± 0.3	37.0 ± 0.6	47.0 ± 1.0
N	4.2 ± 0.2	4.3 ± 0	1.7 ± 0.1	1.5 ± 0.1
Si	3.7 ± 0.3	3.1 ± 0.4	3.2 ± 0.3	4.6 ± 0.4
Ti	0.4 ± 0.2	0.3 ± 0.2	11.1 ± 0.3	11.7 ± 0.5
Al	< 0.3	< 0.3	3.6 ± 0.6	2.4 ± 0.3
F	0.3 ± 0.1	< 0.2	9.0 ± 0.4	1.9 ± 0.2

Table 4.48. XPS results (atomic %) for both failure surfaces in the interfacial failure region for lap specimens thermally treated at 399°C for 2.0 hours, in air. Standard deviations are reported at the 95% confidence limit.

Element	Adhesive failure (interfacial)	
	Side A	Side B
C	26.6 ± 1.9	31.3 ± 8.1
O	40.4 ± 2.8	46.7 ± 5.5
N	1.4 ± 0	1.2 ± 0.1
Si	4.6 ± 0.3	5.4 ± 0.5
Ti	10.9 ± 0.2	11.5 ± 1.6
Al	4.1 ± 0.3	2.1 ± 0.2
F	11.9 ± 0.8	1.8 ± 0.5

Table 4.49. XPS results (atomic %) for both failure surfaces in the interfacial failure region for lap specimens thermally treated at 399°C for 3.0 hours, in air. Standard deviations are reported at the 95% confidence limit.

Element	Adhesive failure (interfacial)	
	Side A	Side B
C	18.1 ± 4.5	24.4 ± 11.8
O	36.9 ± 1.0	48.2 ± 8.2
N	0.9 ± 0.2	1.0 ± 0.4
Si	6.1 ± 0.6	6.7 ± 0.6
Ti	11.2 ± 1.2	13.1 ± 3.9
Al	5.0 ± 0.3	2.4 ± 0.1
F	21.8 ± 2.9	4.2 ± 1.0

at concentration levels that are indicative of failure within the adhesive. Only the specimen thermally treated at 350°C for 11.0 hours showed a slightly higher concentration of silicon on Side B failure surface. The shapes of carbon (C 1s), oxygen (O 1s), nitrogen (N 1s), and silicon (Si 2p) XPS photopeaks in the cohesive failure regions are indicative of polyimide adhesive. Representative XPS spectra for the C 1s, O 1s, N 1s, and Si 2p peaks from a cohesive failure region, from both failure surfaces, for a lap specimen thermally treated at 371°C for 3.0 hrs in air are shown in Figures 4.75 and 4.76.

The XPS results in the interfacial failure regions reveal significant amounts of titanium, aluminum, fluorine, and oxygen (which are all primarily associated with oxide), in addition to smaller amounts of carbon, nitrogen and silicon (which are all primarily associated with the FM-5 adhesive) on both failure surfaces. Representative XPS spectra for the C 1s, O 1s, N 1s, Si 2p, Ti 2p, Al 2p, and F 1s levels from interfacial failure region, from both failure surfaces, for a lap specimen thermally treated at 371°C for 3.0 hrs in air are shown in Figures 4.77 – 4.80. The shape of carbon (C 1s), nitrogen (N 1s) and silicon (Si 2p) XPS photopeaks in the interfacial failure regions are indicative of polyimide adhesive, and the shape of titanium (Ti 2p), aluminum (Al 2p) and fluorine (F 1s) XPS photopeaks are indicative of anodic oxide. The shape of oxygen (O 1s) XPS photopeak in the interfacial failure region is indicative of anodic oxide (primarily TiO<sub>2</sub>) as well as of polyimide adhesive. In general, as the treatment time is increased the amounts of titanium, aluminum, fluorine, and oxygen increase, and those for carbon and nitrogen decrease on both failure surfaces (see Tables 4.31 - 4.49). The XPS data are consistent with the SEM results for oxide failure region. The oxide failure surface was increasingly smoother and was completely covered by an oxide coating as the thermal treatment time was increased at any given treatment temperature. These data support the notion that interfacial failure occurs within the oxide layer, rather than at the interface between the adhesive and oxide coating. In general, for each set of XPS failure analysis results, failure surface Side A exhibits a greater concentration of fluorine and aluminum, while the content of oxygen is significantly greater; titanium is slightly greater on the Side B failure surfaces. The non-equivalent nature of the respective failure

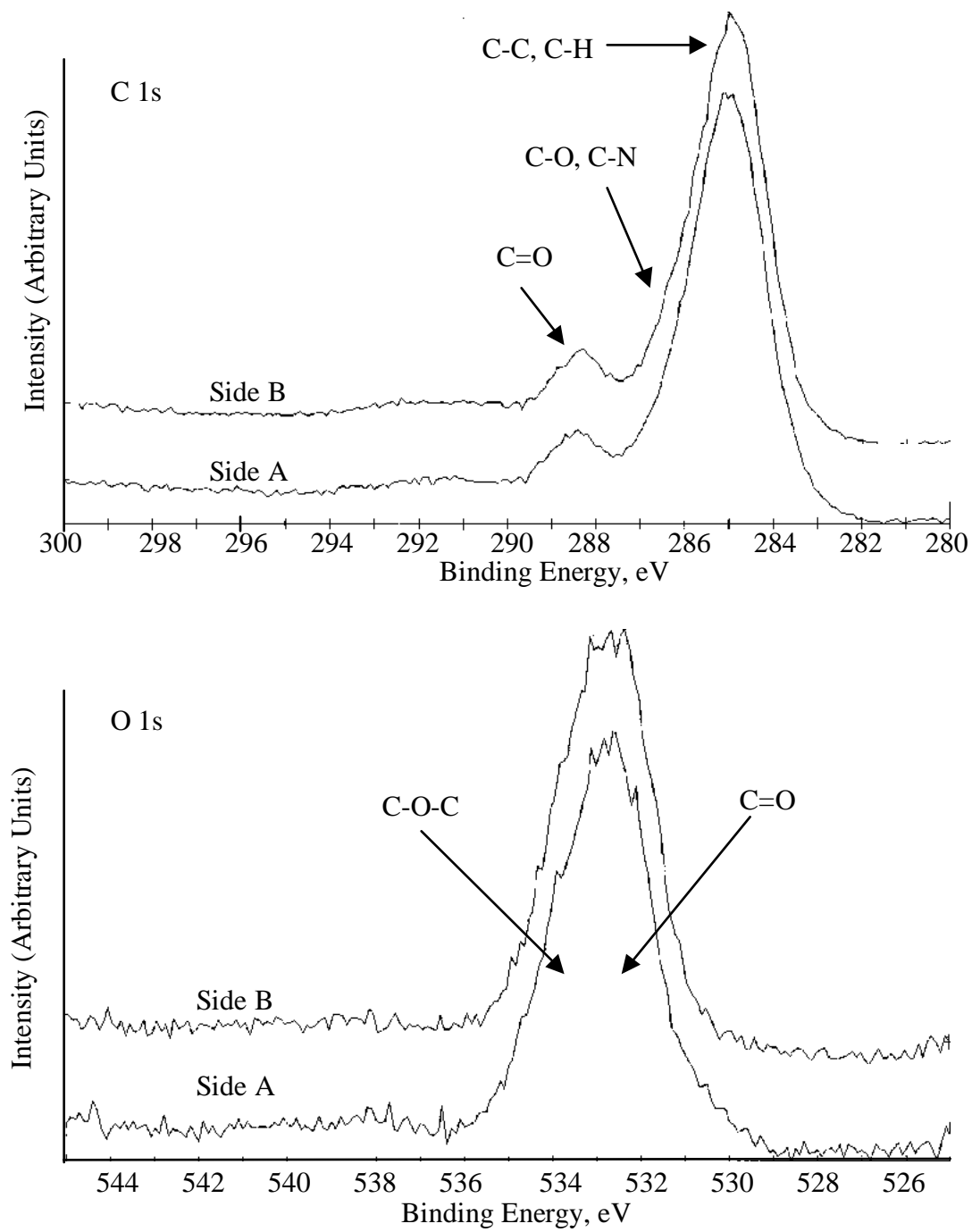


Figure 4.75. Carbon (C 1s) and oxygen (O 1s) XPS photopeaks for Side A and Side B failure surfaces, in cohesive failure region, for a lap specimen thermally treated at 371°C for 3.0 hours in air.

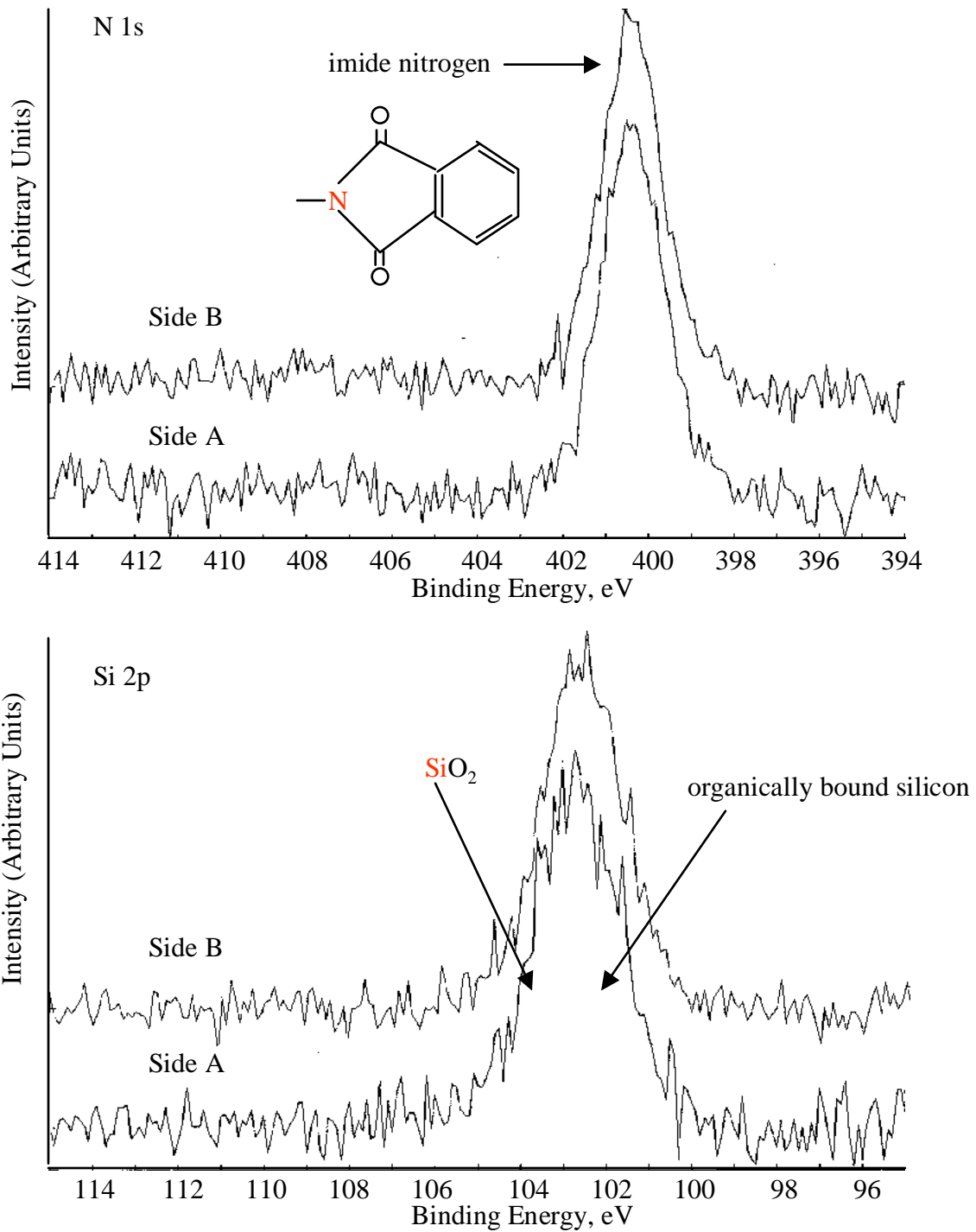


Figure 4.76. Nitrogen (N 1s) and silicon (Si 2p) XPS photopeaks for Side A and Side B failure surfaces, in cohesive failure region, for a lap specimen thermally treated at 371°C for 3.0 hours in air.

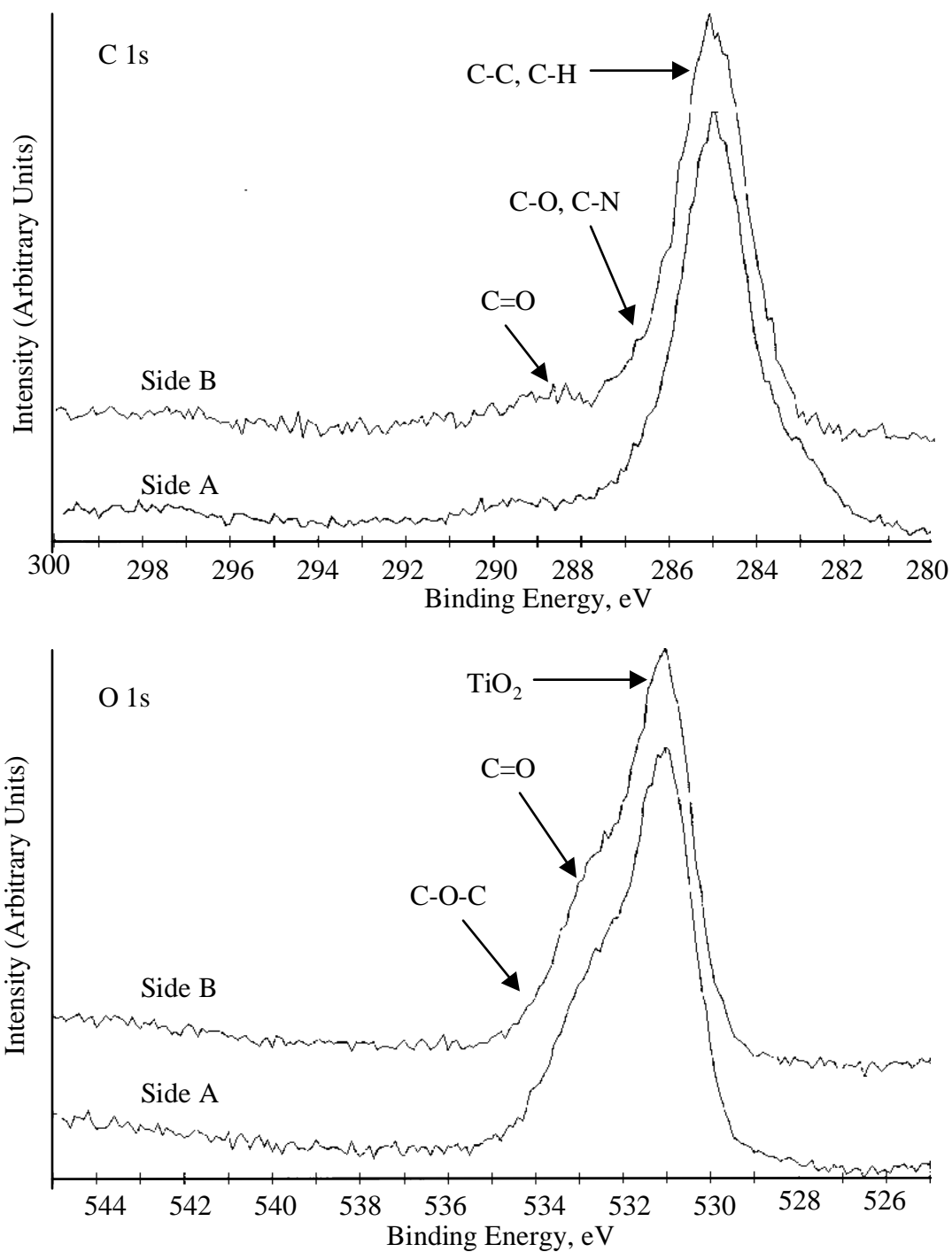


Figure 4.77. Carbon (C 1s) and oxygen (O 1s) XPS photopeaks for Side A and Side B failure surfaces, in interfacial failure region, for a lap specimen thermally treated at 371°C for 3.0 hours in air.

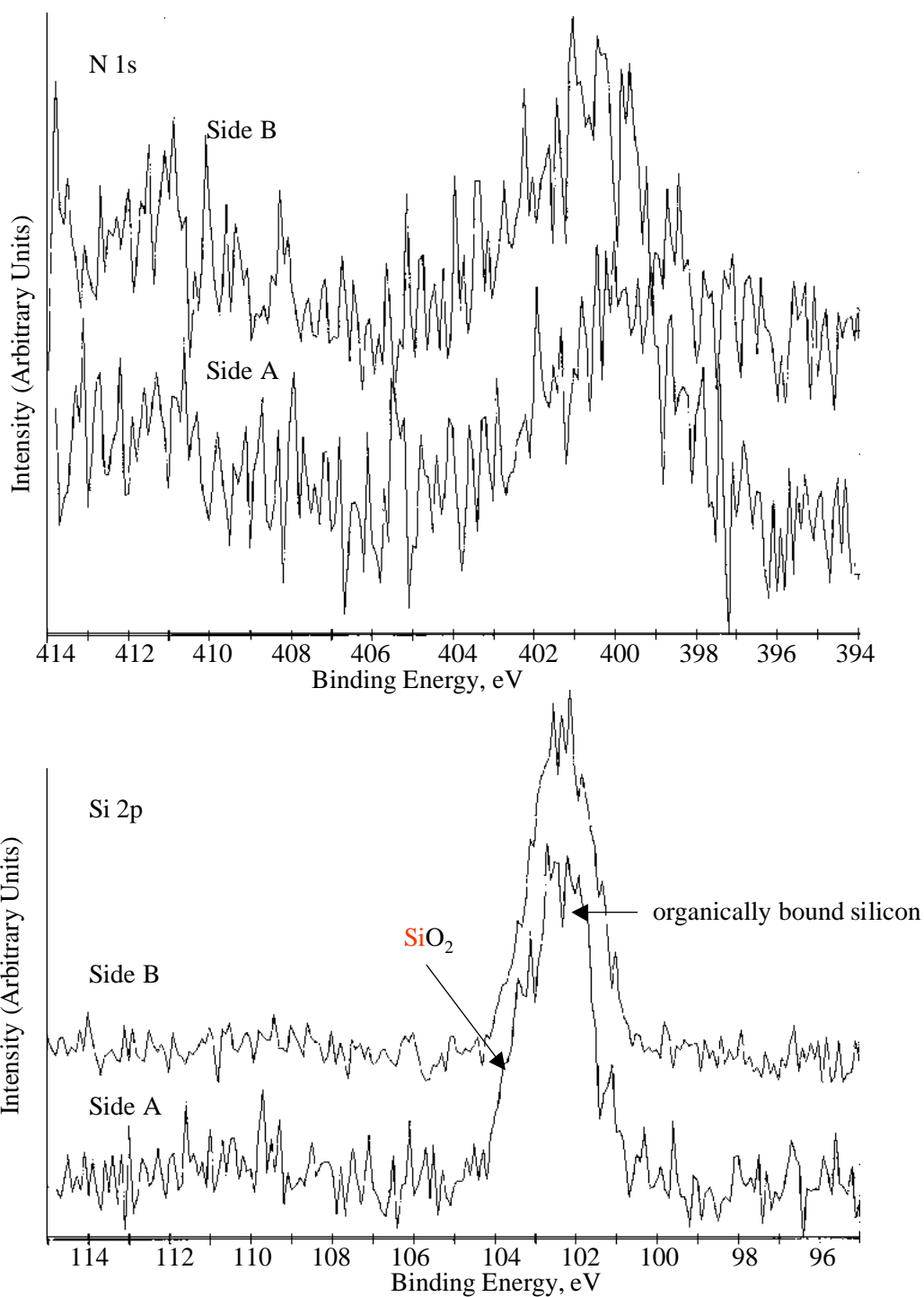


Figure 4.78. Nitrogen (N 1s) and silicon (Si 2p) XPS photopeaks for Side A and Side B failure surfaces, in interfacial failure region, for a lap specimen thermally treated at 371°C for 3.0 hours in air.

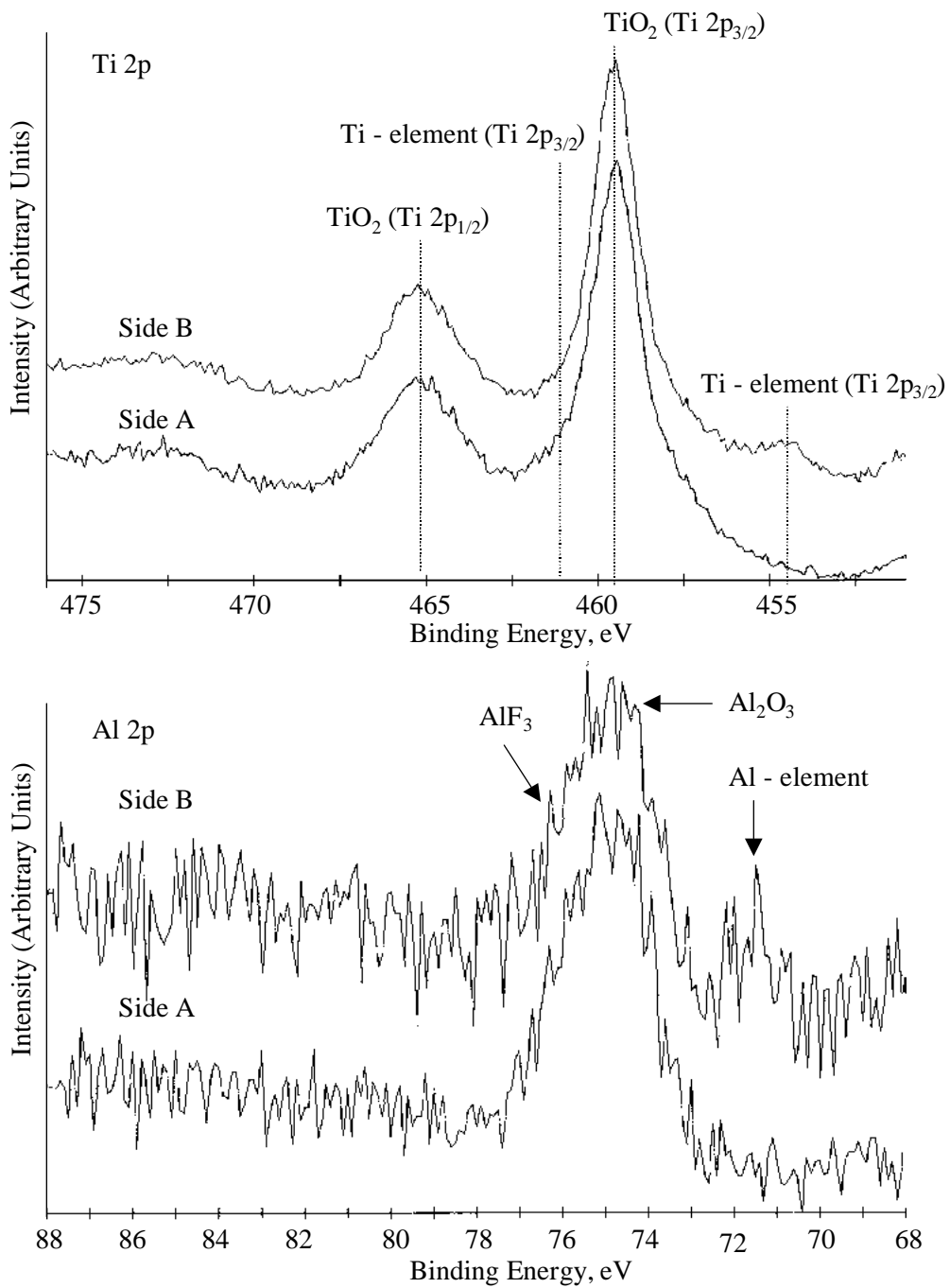


Figure 4.79. Titanium (Ti 2p) and aluminum (Al 2p) XPS photopeaks for Side A and Side B failure surfaces, in interfacial failure region, for a lap specimen thermally treated at 371°C for 3.0 hours in air.

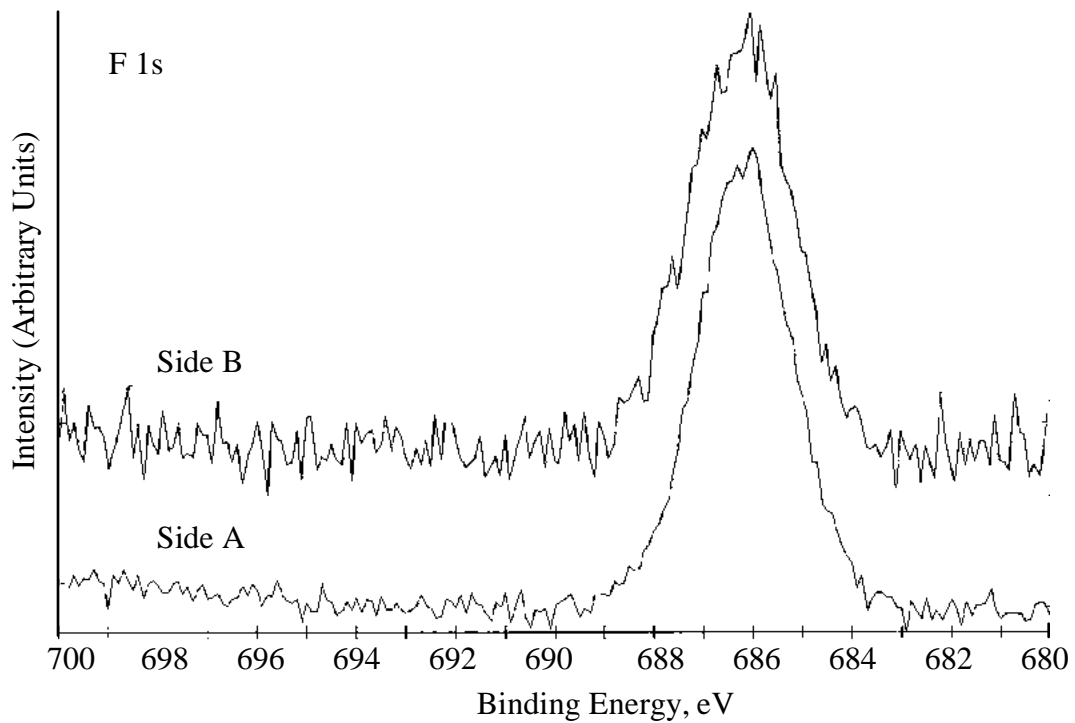


Figure 4.80. Fluorine (F 1s) XPS photopeaks for Side A and Side B failure surfaces, in interfacial failure region, for a lap specimen bonded and thermally treated at 371°C for 3.0 hrs in air.

surfaces indicates that failure is promoted in a boundary region where one domain is rich in aluminum fluoride along with titanium oxide, and the other region is characterized by titanium and aluminum oxides with smaller contributions from fluorine-containing components (principally with aluminum).

The binding energy of titanium, in the interfacial failure regions, suggests that titanium is present as a titanium(IV) oxide on both Side A and Side B failure surfaces (see Figure 4.79). Ti 2p XPS photopeaks for Side B failure surfaces suggest that the oxide coating is very thin (5-10 nm); a small peak is observed for elemental titanium at around 454 eV. Al 2p XPS photopeaks for Side B failure surfaces also show a small peak (barely visible due to signal-noise) for elemental aluminum (~72 eV), for example see Figure 4.79. The measured binding energies for aluminum suggest that aluminum is present not only in an oxide form but also as fluoride, for example, see Figure 4.81 which shows the curve-fit analyses for aluminum photopeaks for a specimen thermally treated at 371°C for 3.0 hrs in air. The curve fit analyses for the fluorine photopeak are consistent with fluorine as an adsorbed fluoride and as fluoride in aluminum fluoride. See Figure 4.82 which shows the curve-fit analyses for fluorine photopeaks for a specimen thermally treated at 371°C for 3.0 hrs in air. The binding energies for aluminum and fluorine as fluoride from the curve fit results were  $76.2 \pm 0.2$  eV and  $686.6 \pm 0.2$  eV, respectively. These binding energies are in good agreements with the reported values for aluminum and fluorine in  $\text{AlF}_3$  [207, 208]. These findings are similar to the results discussed earlier in the analysis of failure surfaces from the wedge specimen durability tests. It was also noted that the amount of “aluminum fluoride” on the failure surfaces increased with increasing treatment temperature and duration of treatment. The presence of fluorine and aluminum fluoride in significant concentrations on the interfacial failure surfaces suggests that the formation of an “aluminum fluoride” is associated with the degradation and debonding process for bonded lap shear specimens treated at elevated temperatures.

The high-temperature studies were carried out in the temperature range 350°C to 399°C, for a much shorter time, 0.5 hour to 3 hours (24 hours only at 350°C), in air. At this treatment

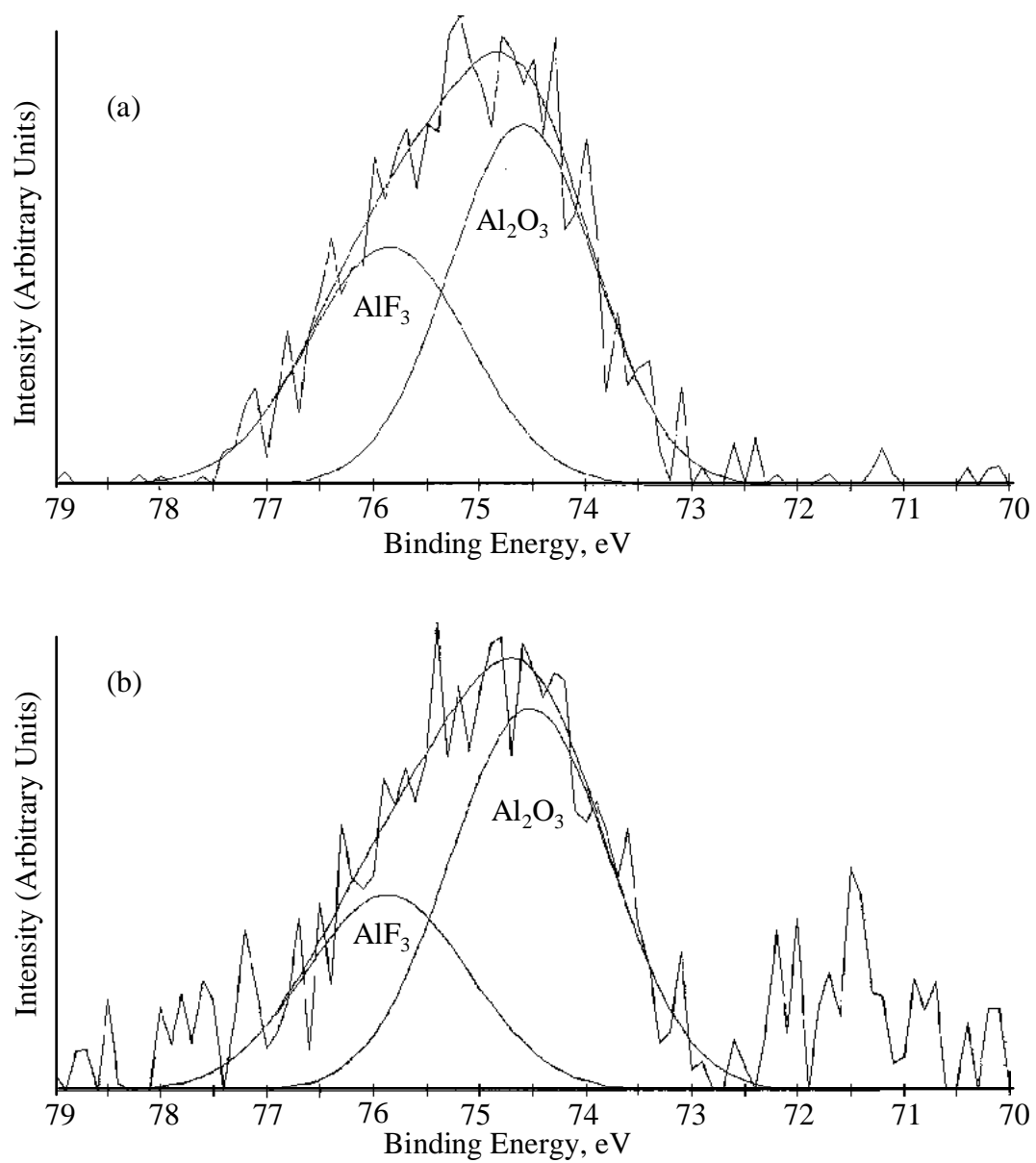


Figure 4.81. Curve-fit XPS analysis of aluminum 2p photopeak in an interfacial failure region for a lap specimen bonded and thermally treated at 371°C for 3.0 hrs in air; (a) Side A failure surface (b) Side B failure surface.

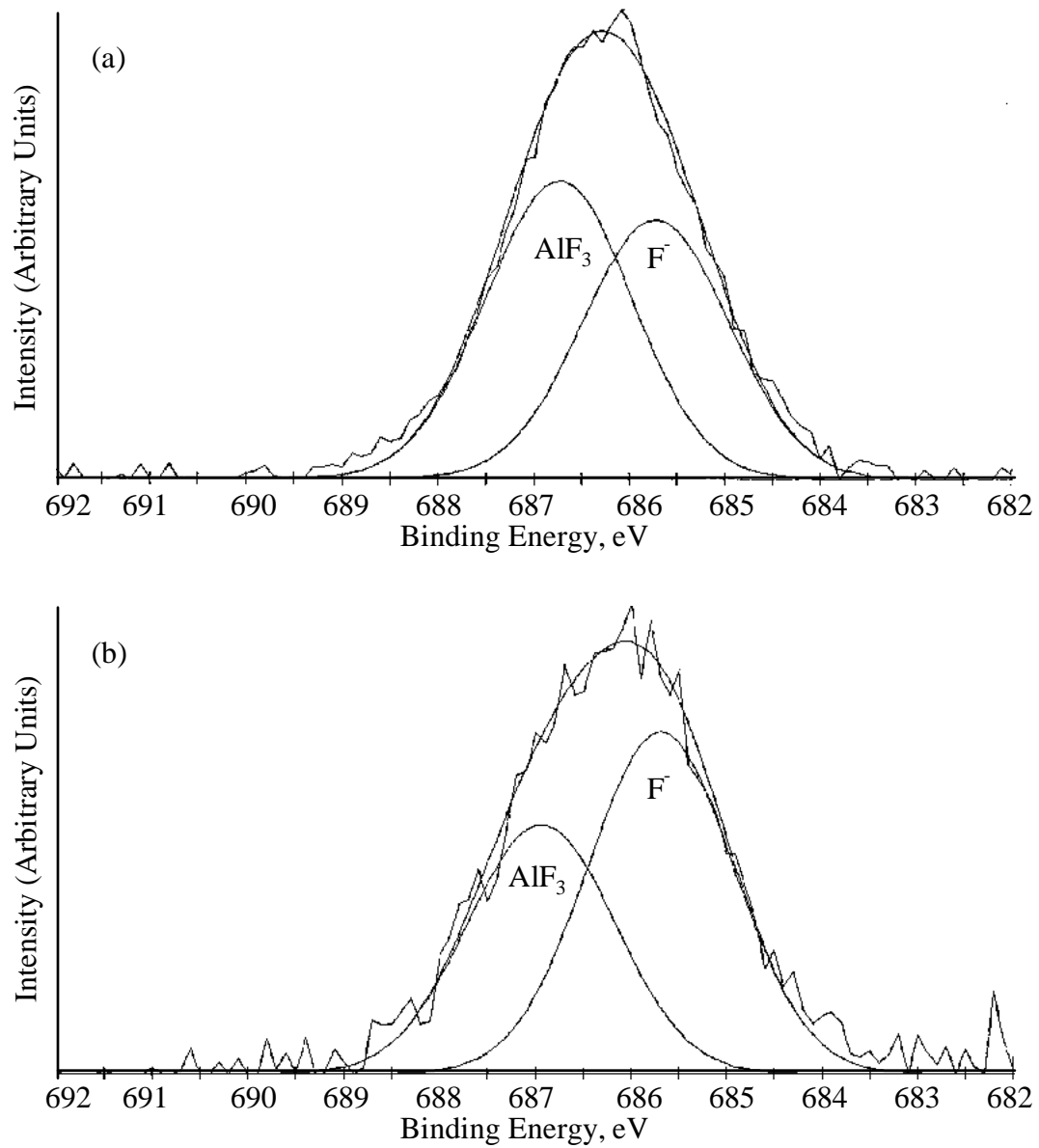


Figure 4.82. Curve-fit XPS analysis of fluorine 1s photopeak in an interfacial failure region for a lap specimen bonded and thermally treated at 371°C for 3.0 hrs in air; (a) Side A failure surface (b) Side B failure surface.

temperature and experimental time scale, the extent of oxygen dissolution into the metal is not large enough to cause any significant decrease in oxide strength. As discussed before, the metal/oxide interface is sharp and no significant tail of the oxygen signal is observed in an Auger sputter-depth profile for a thermally treated (at 371°C in air for up to 3.0 hrs) CAA Ti-6Al-4V alloy. However, the XPS and AES characterization results suggest that failure takes place within the anodic oxide coating, primarily near the oxide/metal interface. The XPS results for the interfacial failure region reveal significant amounts of titanium, aluminum, fluorine and oxygen, in addition to smaller amounts of carbon, nitrogen and silicon. The presence of adhesive as well as fluorine in the oxide coating on both failure surfaces suggests that the locus of failure is not at the oxide/metal interface. Recall that one failure surface (Side A) has relatively larger amounts of aluminum and fluorine compared with the other failure surface, side B. Side A has a relatively thicker oxide coating on top of the adhesive film and side B has a very thin oxide coating (5-10 nm). For example, the AES sputter depth profile results of failure surfaces for a lap specimen thermally treated at 399°C for 3 hrs in air are shown in Figure 4.83. Since a metal surface is easily oxidized upon exposure to air, a thin oxide layers on the metal side (side B) of the failure surface may indicate bond failure at the metal/oxide interface. The fact that the XPS surface analysis reveals fluorine (one of the chemical constituents of the CAA oxide coating) on side B indicates that failure is definitely in the anodic oxide. The AES sputter-depth profile of side A indicates a relatively thick oxide coating on the adhesive film. However, the oxide/adhesive interface is not sharp. The presence of carbon in the oxide layer indicates good wetting of the porous oxide by the adhesive film during the bonding process.

#### 4.4.2.3 Kinetics of Lap-joint Failure

In the thermal treatment studies, it was reasoned that the formation of aluminum fluoride species weakens the oxide and promotes failure within the anodic oxide coatings. Therefore, it is meaningful to follow the reaction kinetics for the formation of aluminum fluoride species. The binding energies for fluorine and aluminum as aluminum fluorides are different from what they would be as adsorbed ions and oxide, respectively. Thus, fluorine and/or aluminum with their

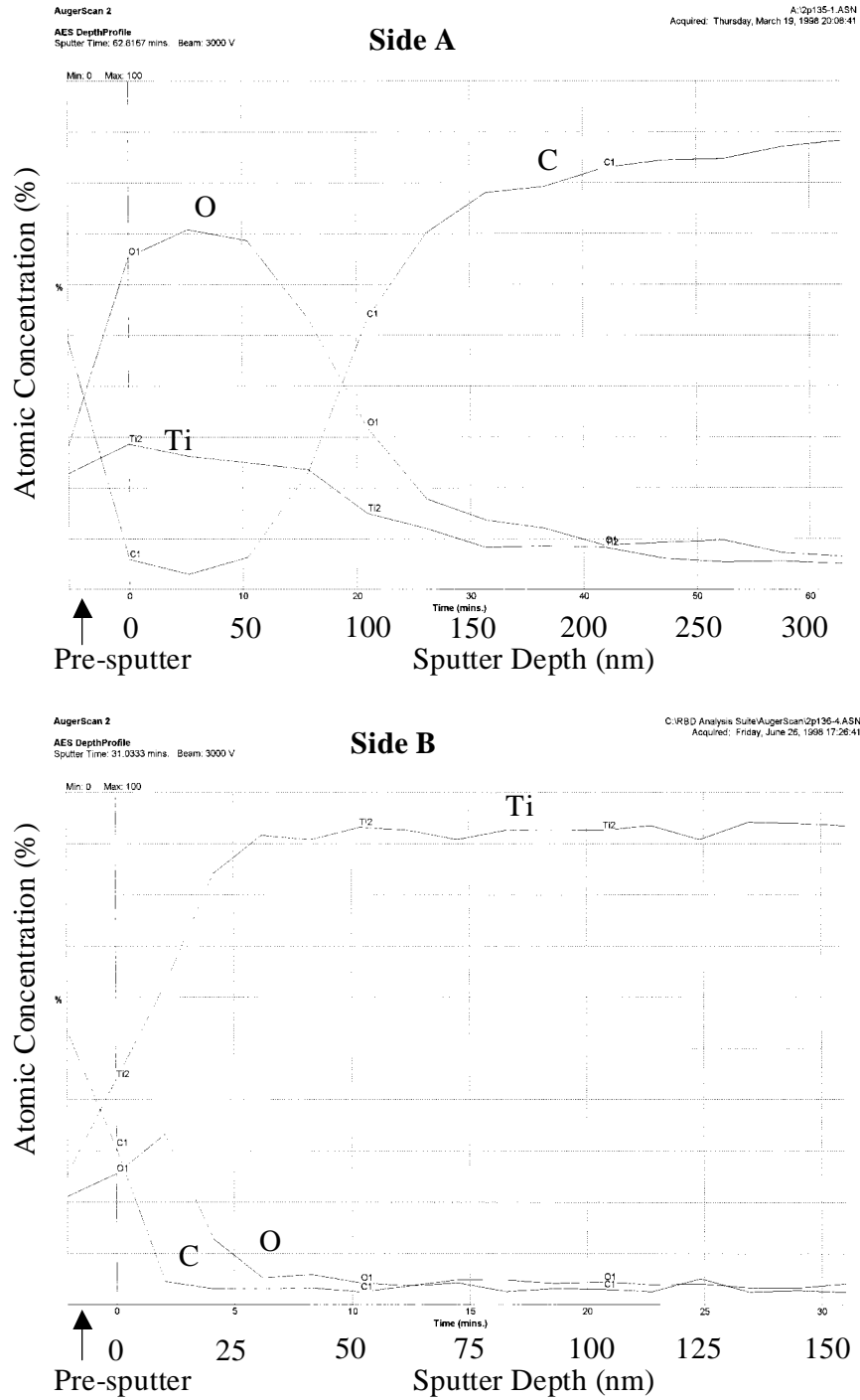


Figure 4.83. Auger sputter-depth profiles of Side A and Side B failure surfaces for a lap specimen thermally treated at 399°C for 3.0 hrs in air.

characteristic photopeak position in aluminum fluoride can be used as fingerprints to follow the reaction kinetics of aluminum fluoride. By plotting the concentration of fluorine or aluminum as fluorides versus thermal treatment time at various temperatures, the rate of aluminum fluoride formation is obtained at the respective temperatures. The activation energy ( $E_a$ ) for the formation of the aluminum fluoride species is then determined from the slope of the Arrhenius plot ( $\log(\text{reaction rate})$  vs.  $1/T$ ).

The average concentration of fluorine, as aluminum fluoride, on the failure surfaces of thermally treated lap specimens is determined from the XPS curve-fit analysis of the fluorine photopeak. Similarly, the average concentration of aluminum, as aluminum fluoride, on the failure surfaces of thermally treated lap specimens is determined from the XPS curve-fit analysis of the aluminum photopeak. XPS test results from only side A of the failure surfaces were used for studying aluminum fluoride reaction kinetics. The reaction rate data for the formation of aluminum fluoride species using fluorine and aluminum as fingerprint elements are shown in Figures 4.84 and 4.85. With just four data points at each temperature, it is difficult to determine, with a good degree of confidence, the rate law for the reaction. However, data for the formation of aluminum fluoride species fit reasonably well ( $R^2 \geq 0.90$ ) a linear reaction rate equation of the form  $y = kt + c$ , where  $y$  is the concentration of fluorine or aluminum as aluminum fluoride;  $k$  is the reaction rate constant;  $t$  is the elapsed time of the reaction (thermal treatment time); and  $c$  is a constant. The first order reaction rate constants, as determined from linear plots of aluminum and fluorine kinetics data at various temperatures, are listed in Table 4.50. The rate of aluminum fluoride formation as a function of treatment temperature in the form of an Arrhenius plot is shown in Figure 4.86. The activation energy values obtained from Arrhenius plots using aluminum and fluorine kinetic data are about the same. The average activation energy for the formation of aluminum fluoride species is approximately 149 kJ/mole. The high activation energy suggests that the rate of aluminum fluoride formation is substantial only at high temperatures.

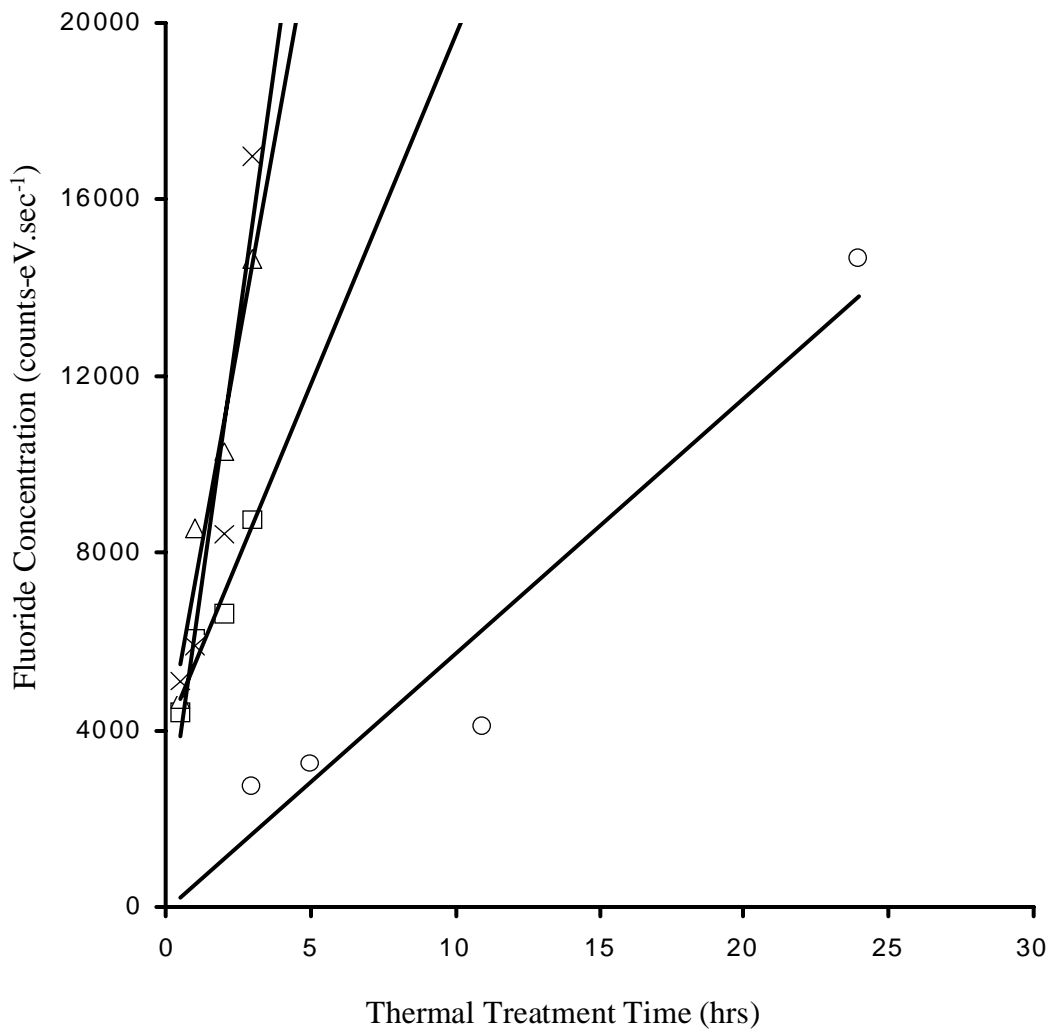


Figure 4.84. Concentration of fluorine, as fluoride, plotted vs. the thermal treatment time at various treatment temperatures: (o) 350°C, (□) 371°C, (Δ) 385°C and (×) 399°C; straight lines are the least-squares fits from the regression analyses.

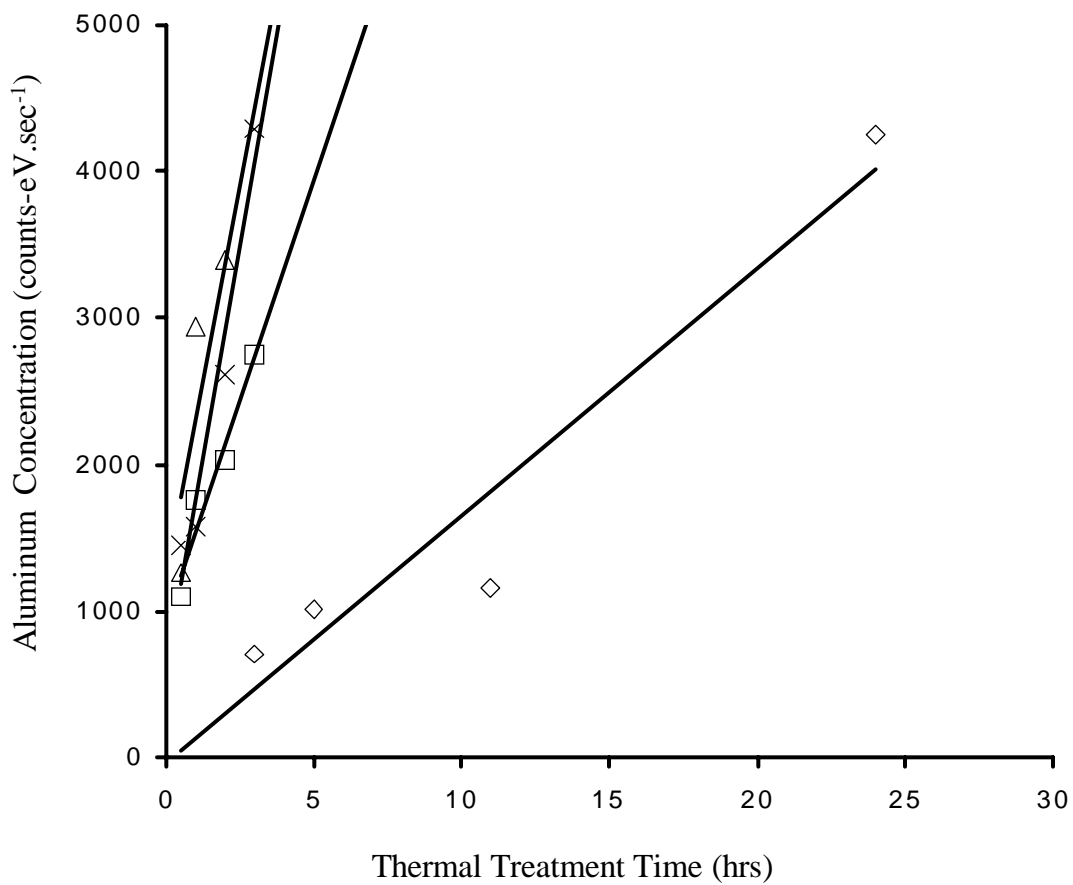


Figure 4.85. Concentration of aluminum, as fluoride, plotted vs. the thermal treatment time at various treatment temperatures: (◇) 350°C, (○) 371°C, (△) 385°C and (×) 399°C; straight lines are the least-squares fits from the regression analyses.

Table 4.50. Linear rate constants for the aluminum – fluorine reaction.

Temperature (°C)	Fluorine (cts-eV.sec <sup>-1</sup> .hr <sup>-1</sup> )	Aluminum (cts-eV.sec <sup>-1</sup> .hr <sup>-1</sup> )
350	579	169
371	1574	601
385	3627	1065
399	4641	1156

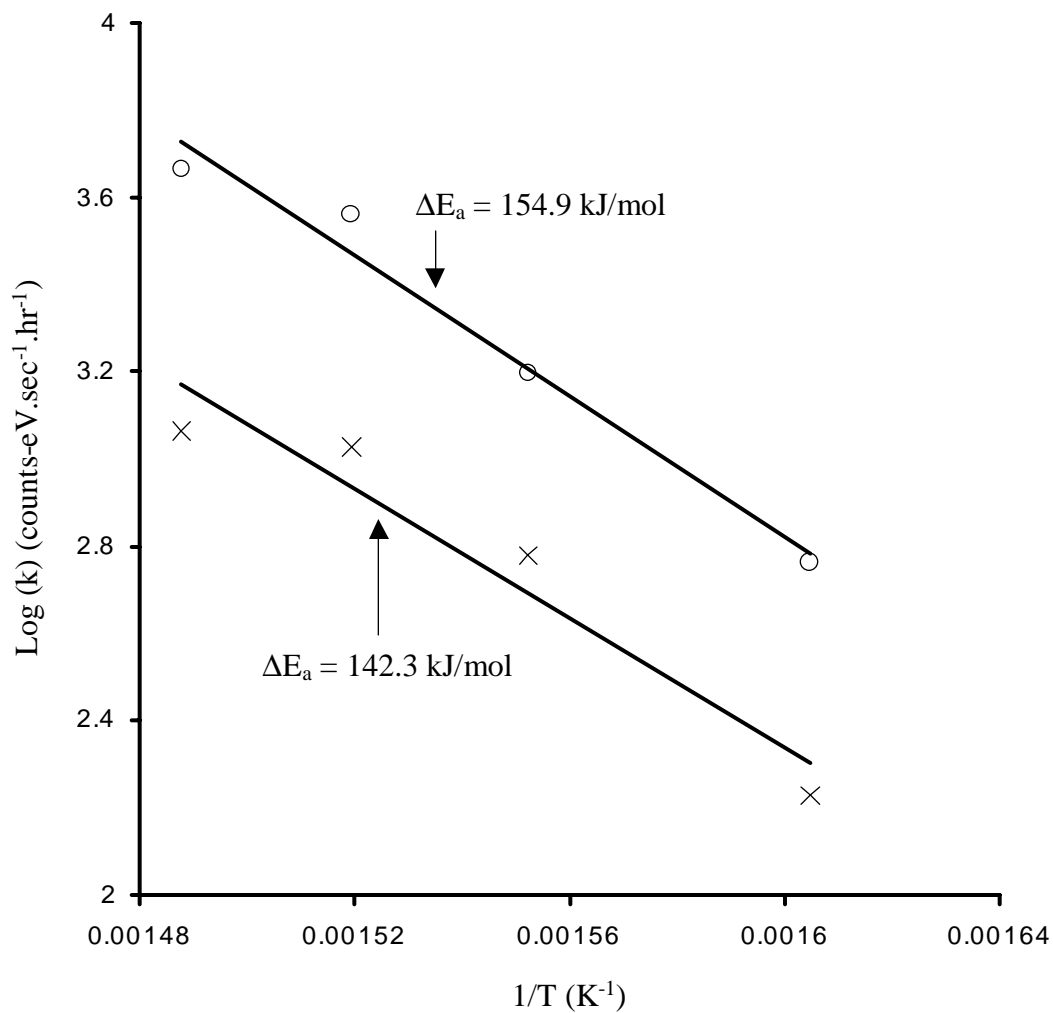


Figure 4.86. Arrhenius plot: rate of aluminum fluoride formation vs.  $1/T$  : (o) linear rate constants from fluorine kinetic data; (x) linear rate constants from aluminum kinetic data; straight lines are the least-squares fits from the regression analyses.

As discussed in the wedge test results, both aluminum oxide and aluminum metal could react with hydrofluoric acid to produce aluminum fluoride. However, the reaction between aluminum metal and hydrofluoric acid is thermodynamically more favorable (see Table 2.1). For thermally treated lap specimens, the failure in the oxide coating always occurred close to the oxide/alloy interphase. This would then suggest that the reaction between aluminum metal and hydrofluoric acid at the oxide/alloy interphase is significant. Recognizing that failure occurred near/or at the oxide/alloy interphase, it is reasoned that the activation energy value obtained for the formation of aluminum fluoride species is more likely that for a reaction between aluminum metal and hydrofluoric acid.

## Chapter 5. Conclusions and Summary

The chromic acid anodization of Ti-6Al-4V alloy produces a porous oxide morphology. The average oxide thickness for CAA Ti-6Al-4V alloy (5 Volts, 20 minutes) is  $45 \pm 5$  nm. The porous oxide morphology is retained by CAA Ti-6Al-4V alloy when it is thermally treated in air at  $371^\circ\text{C}$  for up to 24 hours. The thermally treated CAA Ti-6Al-4V alloy exhibits an increase in oxide thickness (due to thermal oxidation of the alloy) and a slight thickening in the oxide cell-wall. When immersed in boiling water for up to 15 hours, the basic porous nano-rough oxide morphology is retained by CAA Ti-6Al-4V alloy. The boiling water-treated CAA Ti-6Al-4V alloy exhibits a great degree of hydroxylation of the oxide surface. The relative extent of surface hydroxylation varies in the manner 192 hrs treatment > 0.5 hr treatment > non-treated  $\approx$  thermally treated ( $371^\circ\text{C}/3\text{hrs}/\text{air}$ ). The boiling water treated CAA oxide surface produces a relatively non-uniform rough oxide morphology on a micrometer scale, which is attributed to stress induced cracking and spalling of the oxide coating.

The wedge test results show excellent durability in air for CAA Ti-6Al-4V alloy, adhesively bonded with FM-5 polyimide adhesive, in the temperature range  $-25^\circ\text{C}$  to  $177^\circ\text{C}$ . From the average crack length versus exposure time data, the bond durability follows the order  $-25^\circ\text{C} > 24^\circ\text{C} > 177^\circ\text{C}$ . Irrespective of the temperature of exposure, bonded joints failed cohesively at the scrim cloth/adhesive interface in each case. The decrease in bond durability at elevated temperatures is attributed to polymer chain-breaking and visco-elastic effects.

From the average crack length vs. boiling water exposure time data, no significant differences are observed in durability for specimens that are thermally treated, bonded (heat & bond) and then immersed in boiling water compared to non-thermally treated specimens. Wedge specimens that are bonded, thermally treated (bond & heat) at  $371^\circ\text{C}$  for 0.5 hour and 1.0 hour, and then immersed in boiling water also exhibit durability similar to that by the non-thermally treated specimens. In each case, the bonded joint fails cohesively within the adhesive and specifically at the scrim cloth/adhesive interface. The crack propagation is entirely within the adhesive in

boiling water test, and is attributed primarily to water induced plasticization of FM-5 adhesive at the crack tip. For wedge specimens that are bonded and thermally treated (bond & heat) at 371°C for 3 hours, the joint fails in the anodic oxide immediately upon the wedge insertion. Based on the surface analysis results and thermodynamic considerations, it is reasoned that oxide failure in the durability tests is due to the formation of an aluminum fluoride which destroys the integrity of the CAA anodic oxide. The degradation occurs in the bonded specimens during the “bond/heat” thermal treatments.

The durability of as-bonded (non-treated) CAA Ti-6Al-4V wedge specimen in boiling water is in sharp contrast with that in dry atmosphere at elevated temperatures, especially since crack propagation in each case is entirely within the adhesive. Wedge specimens immersed in boiling water show a significant decrease in bond durability, i.e., higher crack growth and lower strain energy release rate, in a relatively very short time (~150 hrs) compared to wedge specimens kept in a forced-air oven at 177°C. These results suggest that, for Ti/FM-5 bonded joints, the boiling water environment is much more severe than a high temperature (< 177°C) dry air environment.

The lap shear specimens that are thermally treated at 177°C and 204°C for various times fail primarily within the adhesive. The lap shear specimens that are thermally treated in air at 177°C for 4 months and at 204°C for 4 weeks exhibit a small loss (9 to 10%) in lap-shear failure strengths compared to non-treated lap specimen (failure strength = 49.5 MPa), the loss in strength is most likely due to chemical degradation (e.g., chain scissions via thermal oxidation) and visco-elastic effects of the FM-5 adhesive.

For lap specimens that are thermally treated at higher temperatures (350°C to 399°C), the principal finding is that the lap-shear failure strength, as well as the extent of cohesive failure within the adhesive, decreases with an increase in thermal treatment-time at a given temperature or with an increase in treatment-temperature at a comparable time. The XPS results for debonded lap specimens suggest that failure is promoted by the formation of an “aluminum fluoride” that results from a reaction of residual fluorine from the anodizing bath and aluminum

alloy. The formation of aluminum fluoride is facilitated by treatment at elevated temperatures. The average activation energy for the formation of aluminum fluoride species is approximately 36 kcal/mole. It is argued that the formation of aluminum fluoride weakens the CAA anodic oxide. A number of reasons for the weakening of the CAA anodic oxide have been suggested: (1) The formation of aluminum fluoride species as a result of reaction between hydrofluoric acid and aluminum oxide introduces large compressive stresses in the oxide due to an increase in the oxide volume. These compressive stresses in the oxide could result in cracking and spalling of the oxide coating under minimal load (mechanically weak oxide film). (2) The fluoride ions could directly react with the metal at the oxide/metal interface to form products at the interface, which could lead to weakening or even debonding of the oxide from the metal (e.g.,  $2\text{Al} + 6\text{HF} = 2\text{AlF}_3 + 3\text{H}_2$ ). (3) Any significant differences in the coefficients of thermal expansion (CTE) between oxides and fluorides could result in a stress build-up inside the oxide when the test sample is cooled after the thermal treatment. Such stresses could promote failure in the oxide.

The dissertation results suggest that adsorbed fluorine in the anodic oxide coatings is detrimental to the bond strength of adhesively bonded Ti-6Al-4V alloy when exposed to elevated temperatures ( $\geq 350^\circ\text{C}$ ).

### **Future Work**

In the current work, it is reasoned that adsorbed fluorine in the anodic oxide coatings is detrimental to the bond strength of adhesively bonded Ti-alloy when exposed to elevated temperatures ( $\geq 350^\circ\text{C}$ ). It was observed that adsorbed fluorine is completely desorbed from the oxide coating when a CAA Ti-6Al-4V alloy specimen is thermally treated at  $371^\circ\text{C}$  in air for as little as 0.5 hr. However, the mechanism by which adsorbed fluorine in the CAA oxide is thermally desorbed is not completely understood. Fluorine when present in the anodic oxide coating purely as HF and/or associated with water, should desorb when the CAA Ti-6Al-4V alloy specimen is thermally treated at  $200^\circ\text{C}$  (pure hydrofluoric acid (HF) boils at  $19.54^\circ\text{C}$ , and  $\text{HF}(35.35\%) + \text{H}_2\text{O}$  boils at  $120^\circ\text{C}$ ). However, the very reason that a temperature higher than

200°C is required to completely desorb fluorine from the CAA oxide coating suggests that during the thermal treatment a part of fluorine reacts with some element(s) such as titanium to form a new fluoride species which is stable up to a certain temperature, after which it thermally decomposes. In the absence of detailed investigation, the chemical nature of the new fluoride species could only be speculated. The new species could be titanium tetrafluoride (TiF<sub>4</sub>). It is known that the reaction between titanium dioxide (TiO<sub>2</sub>) and hydrofluoric acid (HF) to form titanium tetrafluoride is thermodynamically feasible at room temperature, and it is also known that TiF<sub>4</sub> sublimates at about 285°C. This could be a plausible mechanism by which fluorine is removed from the oxide coating of the CAA Ti-6Al-4V alloy when it is heated to 371°C in air. However, a detailed investigation of the mechanism for removal of fluorine from the oxide coating is required to assess the validity of the proposed mechanism.

Another extension of this work would be to investigate the performance of FM-5 bonded to sodium hydroxide anodized (SHA) Ti-alloy. The anodic oxide coating on Ti-6Al-4V alloy could be prepared via sodium hydroxide anodization (SHA), however, unlike CAA oxide coating, fluorine is not incorporated in the oxide coatings. The thermal stability of oxide coatings produced via SHA treated Ti-6Al-4V alloy should be compared with SHA oxide coatings containing fluoride ions. Fluorine could be incorporated into the SHA oxide coating via absorption from solution containing fluoride ions.

## References

1. A.J. Kinloch, “*Adhesion and Adhesives Science and Technology*,” Chapman and Hall, New York, 1987, p. 2.
2. B. Dattaguru, R.A. Everett, Jr., J.D. Whitcomb and W.S. Johnson, *J. Eng. Mat. Technol.* **106**, 59 (1984).
3. A. Stevenson and E.H. Andrews, in “*Adhesion 3*”, ed. K.W. Allen., Applied Science Publishes, Essex, England, 1982, p. 56.
4. J.M. Park and J.P. Bell, *Adhesion Aspects of Polymeric Coatings*, ed. K.L. Mittal, Plenum Press, New York, 1983, p. 205.
5. G.W. Critchlow and D.M. Brewis, *Int. J. Adhes. Adhes.*, **15**, 161 (1995).
6. R.P. Digby and D.E. Packham, *Int. J. Adhes. Adhes.*, **15**, 61 (1995).
7. H.M. Clearfield, D.K. Shaffer, S.L. Vandoren, and J.S. Ahearn, *J. Adhes.*, **29**, 81 (1989).
8. H.M. Clearfield, D.K. Shaffer, J.S. Ahearn, and J.D. Venables, *J. Adhes.*, **23**, 83 (1987).
9. D.K. Shaffer, H.M. Clearfield, C.P. Blankenship, and J.S. Ahearn, *In Proceedings of the 19<sup>th</sup> SAMPE Technical Conference*, Society for the Advancement of Material and Process Engineering, 1987, p. 291.
10. A.J. Kinloch and N.R. Smart, *J. Adhes.*, **12**, 23 (1981).
11. A.J. Kinloch, H.E. Bishop, and N.R. Smart, *J. Adhes.*, **14**, 105 (1982).
12. A.J. Kinloch, *Adhesion-6*, ed. K.W. Allen, Applied Science Pub., London, 1982, p. 95.
13. A. Datta, R.A. Pethrick, and S. Affrossman, *J. Adhes.*, **15**, 13 (1982).
14. T.S. Sun, J.M. Chen, J.D. Venables, and R. Hopping, *Appl. Surf. Sci.*, **1**, 202 (1978).
15. D. Trawinski, S. Kodali, R. Curley, D.K. McNamara, and J.D. Venables, In “*Proceedings of the 14<sup>th</sup> National SAMPE Technical Conference*”, Society for the Advancement of Material and Process Engineering, 1983, p. 114.
16. J.D. Venables, D.K. McNamara, J.M. Chen, T.S. Sun, and R.L. Hopping, *Appl. Surf. Sci.*, **3**, 88 (1979).
17. J. Sanchez and J. Augustynski, *J. Electroanal. Chem.*, **103**, 423 (1979).
18. R.D. Shannon and C.T. Prewitt, *Acta Crystallogr. Sect. B*, **B25**, 925 (1968).

19. Materials Science and Technology Series; *Inorganic Solid Fluorides, Chemistry and Physics*, ed. P. Hagemuller, Academic Press, Inc., London, 1985, p.5.
20. P.W. Kirklin, P. Auzins, and J.E. Wertz, *J. Phys. Chem. Solids*, **26**, 1067 (1965).
21. J.W. McBain and D.G. Hopkins, *J. Phys. Chem.* **29**, 88 (1925).
22. A.J. Kinloch, *J. Mater. Sci.* **15**, 2141 (1980).
23. E.M. Boroff and W.C. Wake, *Trans. Inst. Rubber Industry*, **25**, 199 (1949).
24. D.E. Packam in “*Aspects of Adhesion 7*”, D.J. Alner and K.W. Allen, ed., Transcript Books, London, 1973, p. 68.
25. K. Kato, *Polymers*, **8**, 33 (1967).
26. K. Kato, *Polymer*, **9**, 419 (1968).
27. D.J. Arrowsmith, *Trans. Inst. Metal Finish*, **48**, 88 (1970).
28. D. Tabor and R.H.S Winterton, *Proc. Roy. Soc.*, **A312**, 435 (1969).
29. J.N. Israelachvili and D. Tabor, *Proc. Roy. Soc.*, **A331**, 19 (1972).
30. F.M. Fowkes, *Physicochemical Aspects of Polymer Surfaces*, Vol. **2** (ed. K.L. Mittal), Plenum, New York, , 1983, p. 583.
31. R.J. Good, *Treatise on Adhesion and Adhesives*, Vol. 1, ed. R.L. Patrick, Marcel Dekker, New York, 1967, p. 15.
32. L. Pauling, *The Nature of the Chemical Bond*, Cornell University Press, New York, 1960, p. 33.
33. M. Gettings and A.J. Kinloch, *J. Mat. Sci.*, **12**, 2511 (1977).
34. M. Gettings and A.J. Kinloch, *Surf. Interface Anal.*, **1**, 189 (1980).
35. W.C. Wake, in *Recent Advances in Adhesion*, ed. L.H. Lee, Gordon and Breach, New York, 1973.
36. J.P. Bell and W.T. McCarvill, *J. Appl. Polymer Sci.*, **18**, 2243 (1974).
37. A.E. Yaniv, I.E. Klein, J. Sharon, and H. Dodiuk, *Surf. Interface Anal.*, **5**, 93 (1983).
38. E.H. Andrew and A.J. Kinloch, *Proc. Roy. Soc.*, **A332**, 385 (1973).
39. E.H. Andrew and A.J. Kinloch, *Proc. Roy. Soc.*, **A332**, 401 (1973).
40. A.N. Gent and A.J. Kinloch, *J. Polymer Sci.*, **A2**, 659 (1971).
41. R.A. Gledhill and A.J. Kinloch, *J. Adhes.*, **6**, 315 (1974).

42. A.J. Kinloch, *J. Adhes.*, **10**, 193 (1979).
43. D.K. Owens, *J. Appl. Polymer Sci.*, **18**, 1869 (1974).
44. D.K. Owens, *J. Appl. Polymer Sci.*, **19**, 265 (1975).
45. D.K. Owens, *J. Appl. Polymer Sci.*, **19**, 3315 (1979).
46. F.M. Fowkes, *Rub. Chem. Technol.*, **57**, 328 (1984).
47. F.M. Fowkes, C.Y. Sun, S.T. Joslin, *Corrosion Control Organic Coatings*, ed. H. Leidheiser, NACE, Houston, Texas, 1981, p.1.
48. S.S. Voyutskii and V.L. Vakula, *J. Appl. Polym. Sci.* **7**, 475 (1963).
49. S.S. Voyutskii, *Adhes. Age*, **5**, 30 (1962).
50. B.V. Deryaguin, *Research*, **8**, 70 (1955).
51. B.V. Deryaguin and V.P. Smilga, *Adhesion, Fundamentals and Practice*, McLaren and Son, London, 1969, p. 152.
52. H. Krupp, *J. Adhes.*, **4**, 83 (1972).
53. H. Krupp, *J. Adhes.*, **5**, 269 (1973).
54. G. H. Harrach and B.N. Chapman, *Thin Solid Films*, **13**, 157 (1972).
55. S.M. Skinner, R.L. Savage, J. Rutzler, *J. Appl. Phys.*, **24**, 439 (1953).
56. P. Commercon and J.P. Wightman, *J. Adhes.*, **22**, 13 (1987).
57. T.A. DeVilbiss, D.L. Messick, D.J. Progar and J.P. Wightman, *Composites*, **16**, 207 (1985).
58. J.A. Filbey, J.P. Wightman, and D.J. Progar, *J. Adhes.*, **20**, 283 (1987).
59. C.U. Ko and J.P. Wightman, *J. Adhes.*, **24**, 93 (1987).
60. F. Bouquet, J.M. Cuntz, C. Coddet, *J. Adhes. Sci. Tech.*, **6**, 233 (1992).
61. H.S. Schwartz, *SAMPE J.*, **13**, 2 (1977).
62. H.M. Clearfield, D.K. McNamara, and G.D. Davis, *Surface Preparation of Metals*, Engineered Materials Handbook, Volume 3, Adhesives and Sealants, ed. H.F. Brinson, ASM International, Materials Park, Ohio, 1990, p. 259.
63. B.L. Holmes, *Effect of Derivatized Oxide Layer and Environment on the Durability of Aluminum and Titanium Bonds*, M.S. Thesis, Virginia Polytechnic Institute and State University, Blacksburg, VA, 1994.

64. J.J. Bickerman, *Appl. Chem.*, **11**, 81 (1961).
65. M.H. Stone, *J. Adhes.*, **26**, 101 (1988).
66. A. Mahoon, in “*Durability of Structural Adhesives*”, ed. A.J. Kinloch, Applied Science Publisher Ltd., Essex, England, 1983, p. 264.
67. B.M. Ditchek, K.R. Breen, T.S. Sun and J.D. Venables in “*Proc. 25<sup>th</sup> Nat. SAMPE Symp.*”, May 1980, p. 134.
68. J.A. Filbey, *Factors Affecting the Durability of Ti-6Al-4V/Epoxy Bonds*, Ph.D. Dissertation, Virginia Polytechnic Institute and State University, Blacksburg, VA, 1987, p. 122.
69. J.D. Venables, *J. Mater. Sci. Technol.*, **19**, 2431 (1984).
70. J.A. Filbey and J.P. Wightman, *J. Adhes.*, **28**, 1 (1989).
71. R.W. Walter, D.L. Voss and M.S. Hochberg, *2<sup>nd</sup> SAMPE Tech. Conf. Series*, **9**, 321 (1970).
72. C.V. Cagle, *Handbook of Adhesive Bonding*, McGraw-Hill, New York, 1973, p. 127.
73. K.B. Dass and J.A. Marceau, *Corrosion*, **30**, 324 (1974).
74. C.L. Hendricks and S.G. Hill, *SAMPE Q.*, **12**, 32 (1981).
75. R.F. Wegman, M.C. Ross, S.A. Slota and E.S. Duda, Picatinny Arsenal Technical Report 4186, 1971.
76. A. Mahoon and J.L. Cotter, *SAMPE Tech. Conf. Series*, **10**, 425 (1978).
77. A. Mahoon, In “*Durability of Structural Adhesives*”, ed. A.J. Kinloch, Applied Science Publication, London, 1983, p. 255.
78. B.M. Ditchek, K.R. Breen, T.S. Sun, and J.D. Venables, in “*Proceeding 25<sup>th</sup> National SAMPE Symp.*”, May 1980, p. 882.
79. G.W. Lively, LTV-Vought Systems Division, Tech. Report AFML-TR-73-270, (1974).
80. B.M. Ditchek, K.R. Breen, T.S. Sun, J.D. Venables, and S.R. Brown, *12<sup>th</sup> National SAMPE Technical Conference* Oct. 7-9, 1980, p. 882.
81. S.R. Brown, *27<sup>th</sup> National SAMPE Symp.* May 4-6, 1982, p. 363.
82. R.F. Wegman, D.W. Levi, *27<sup>th</sup> National SAMPE Symp.*, May 4-6, 1982, p. 440.
83. M.J. Felsen, *SAMPE Tech. Conf. Series*, **10**, 100 (1978).

84. A. J. Kinloch, *J. Mat. Sci.*, **17**, 617 (1982).
85. M.C. Locke, K.M. Harriman, and D.B. Arnold, *25<sup>th</sup> National SAMPE Symp. And Exhib.*, May, 1980, p. 1.
86. J.G. Dillard and I. Spinu, "Plasma Treatment of Composites for Adhesive Bonding," in *How to Apply Advanced Composites Technology, Proceedings of the Fourth Annual Conference on Advanced Composites*, ASM International, 1988, p. 199.
87. R.R. Sowell, N.J. DeLollis, H.J. Gregory and O. Montoya, *J. Adhes.*, **4**, 15 (1972).
88. K. Rossmann, *J. Polym. Sci.*, **19**, 141 (1956).
89. C.A.L. Westerdahl, J.R. Hall, E.C. Schramm and D.W. Levi, *J. Colloid Interface Sci.*, **47**, 610 (1974).
90. N.J. DeLollis, *Rubber Chem. Technol.*, **46**, 549 (1973).
91. H.E. Wechsberg and J.B. Webber, *Mod. Plast.*, **38**, 199 (1961).
92. N.J. DeLollis and O. Montoya, *J. Adhes.*, **3**, 57 (1971).
93. D.K. Owens, *J. Appl. Polym. Sci.*, **19**, 265 (1975).
94. A. Bradley and T.R. Heagney, *Anal. Chem.*, **42**, 894 (1970).
95. A. Baszkin and L. Ter-Minassian-Saraga, *Polymer*, **19**, 1083 (1978).
96. R.H. Hansen and H. Schonhorn, *J. Polym. Sci.*, **B4**, 203 (1966).
97. H. Schonhorn, F.W. Ryan and R.H. Hansen, *J. Adhes.*, **2**, 93 (1970).
98. D.M. Brewis, and D. Briggs, *Polymer* **22**, 7 (1981).
99. B. Westerlind, A. Larsson, and M. Rigdahl, *Int. J. Adhes. Adhes.*, **7**, 141 (1987).
100. H. Yasuda, H.C. Marsh, S. Brandt, and C.N. Reilley, *J. Polym. Chem. Ed.* **15**, 991 (1977).
101. G.D. Davis, P.L. Whisnant, D.K. Shaffer, G.B. Groff, and J.D. Venables, *J. Adhes. Sci. Tech.*, **9**, 527 (1995).
102. J.G. Dillard, F.R. Jackson, B.L. Holmes, L. Aartun, H. Parvatareddy, D.A. Dillard, and R. Zatorski, *J. Adhes.*, **65**, 217 (1998).
103. J.G. Dillard, K.L. Wolfe, and B.L. Holmes, *J. Adhes.*, **62**, 113 (1997).
104. K.L. Wolfe, J.G. Dillard, S.R. Harp, and J.W. Grant, *J. Adhes.*, **60**, 141 (1997).
105. *Handbook of Chemistry and Physics*, D.R. Lide, Editor in Chief, 72<sup>nd</sup> edition, CRC Press, USA, 1991, p. 4-29.

106. R.G. Muraca and J.S. Whittick, *Materials Data Handbook on Titanium 6Al-4V*, NASA Tech Brief B73-10372, October 1973.
107. R.M. Brick, A.W. Pense, and R.B. Gordon, "Structure and Properties of Engineering Materials", 4<sup>th</sup> Edition, McGraw-Hill Book Company, New York, 1977.
108. J.A. Skiles and J.P. Wightman, *J. Adhes.*, **26**, 301 (1988).
109. A.M. Cheng, "Anodic Oxide Formation on Ti-6Al-4V in Chromic Acid for Adhesive Bonding," M.S. Thesis, Virginia Polytechnic Institute and State University, Blacksburg, Virginia, 1983.
110. F. Kover and M.J. Musselin, *Thin Solid Films*, **2**, 211 (1968).
111. N.R. Armstrong and R.K. Quinn, *Surf. Sci.*, **67**, 451 (1977).
112. B.M. Ditchek, K.R. Breen, T.S. Sun and J.D. Venables, in "*Proc. 25<sup>th</sup> Nat. SAMPE Symp.*," May 1980, p. 13.
113. G.D. Davis, M. Natan and K.A. Anderson, *Appl. Surf. Sci.*, **15**, 321 (1983).
114. M. Natan and J.D. Venables, *Electrochem. Soc. Extended Abstract*, **83**, 379 (1983).
115. A.C. Fraker and A.W. Ruff, *Corros. Sci.*, **11**, 763 (1971)
116. M. Natan and J.D. Venables, *J. Adhes.*, **15**, 125 (1983).
117. M. Assefpour-Dezfuly, C. Vlachos, and E.S. Andrews, *J. Mat. Sci.*, **19**, 3626 (1984).
118. C.E. Shamblen and T.K. Redden, in "The Science, Technology and Application of Titanium", R.I. Jaffe and N.E. Promisel, Eds., Pergamon, Oxford, 1966, p. 199.
119. A.M Chaze and C. Coddet, *J. Mat. Sci.*, **22**, 1206 (1987).
120. A.C. Kennedy R. Kohler, and P. Poole, *Int. J. Adhes. Adhes.*, **3**, 133 (1983).
121. B.M. Parker, *J. Adhes.*, **26**, 131 (1988).
122. J. Comyn, "Durability of Structural Adhesives", edited by A.J. Kinloch, Applied Science Publisher, New York, 1983, p. 108.
123. D.M. Brewis, J. Comyn, and R.J.A. Shalash, *Int. J. Adhes. Adhes.*, October, 146 (1982).
124. E.J. Ripling, S. Mostovoy, and C.F. Bersch, *J. Adhes.*, **3**, 145 (1971).
125. J.P. Sargent and K.H.G. Ashbee, *J. Phys. D*, **14**, 1933 (1981).
126. S.R. Brown, *Proc. 27<sup>th</sup> Natl. SAMPE Symp.* , Azusa, CA, 1982, p. 363.
127. R.F. Wegman and D.W. Levi, *Proc. 27<sup>th</sup> Natl. SAMPE Symp.*, Azusa, CA, 1982, p. 440.

128. M. Natan and J.D. Venables and K.R. Breen, *Proc. 27<sup>th</sup> Natl. SAMPE Symp.*, Azusa, CA, 1982, p. 178.
129. C. Matz, *Int. J. Adhes. Adhes.*, **8**, 17 (1988).
130. H. Parvatareddy, “*Durability of Polyimide Adhesives and their Bonded Joints for High Temperature Applications*,” Ph.D. Thesis, Virginia Polytechnic Institute and State University, Blacksburg, Virginia, November, 1997.
131. D.J. Progar, *J. Adhes. Sci. Tech.*, **1**, 135 (1987).
132. H.M. Clearfield, G.O. Cote, K.A. Olver, D.K. Shaffer, and J.S. Ahearn, *Surf. Interface Anal.*, **11**, 347 (1988).
133. D.K. Shaffer, H.M. Clearfield, C.P. Blankenship, Jr., and J.S. Ahearn, *Proc. 19<sup>th</sup> SAMPE Tech. Conf.*, SAMPE, Azusa, CA, 1987, p. 291.
134. D.J. Progar and T.L. St. Clair, *Int. J. Adhes. Adhes.*, **6**, 25 (1986).
135. D.J. Progar and T.L. St. Clair, *J. Adhes.*, **21**, 35 (1987).
136. “Reactivity of Inorganic Substances,” Handbook by R.A. Lidin, V.A. Molochko, L.L. Andreeva, R.A. Lidin ed., Begell House Inc., New York, 1996, p. 283.
137. M.W. Chase Jr., C.A. Davies, J.R.D. Downey Jr., D.J. Frurip, R.A. McDonald and A.N. Syverud, Eds., *JANAF Thermochemical Tables*, 3<sup>rd</sup> edition, American Chemical Society, Washington D.C., 1986.
138. CRC Handbook of Chemistry and Physics, D. R. Lide chief ed., 81<sup>st</sup> Edition, 1999-2000.
139. “Thermochemical Data of Pure Substances,” Ishan Barin, ed., VCH publication, New York, 3<sup>rd</sup> edition., 1995.
140. Materials Science and Technology Series; *Inorganic Solid Fluorides, Chemistry and Physics*, ed. P. Hagenmuller, Academic Press, Inc., London, 1985, p. 579.
141. P.L. Daniel and R. A. Rapp, “*Halogen Corrosion of Metals*”, in: *Advances in Corrosion Science and Technology*, eds. M.G. Fontana and R.W. Staehle, Vol. 5, Plenum Press, New York, 1976, p. 55-172.
142. P.M. Hergenrother, *Trends Polym. Sci.*, **4**, 104 (1996).
143. T.L. St. Clair and D.J. Progar, *J. Adhes.*, **47**, 67 (1984).
144. J.G. Smith and P.M. Hergenrother, *Polymer Pre-prints*, **35**, 353 (1994).

145. C.L. Hendricks and S.G. Hill, in “ Polyimides: Synthesis, Characterization and Applications, Vol. 2, Plenum Press, New York, 1984, p.1103.
146. R.D. Rossi, *Polyimides*, Engineered Materials Handbook, Volume 3, Adhesives and Sealants, H.F. Brinson (Ed.), ASM International, Materials Park, Ohio, 1990, p. 151.
147. J.W. Verbicky, Jr., Encyclopedia of Polymer Science and Engineering, vol. 12, John Wiley and Sons, New York, 1988, p. 364.
148. R.A. Dine-Hart and W.W. Wright, *Makromol. Chem.*, **153**, 237 (1972).
149. V.K. Belyakov, A.A. Kosobutskaya, I.V. Belyakova, M.V. Kozlova and L.B. Sokolov, *Polym. Sci. USSR (Engl. Transl.)*, **15**, 1660 (1973).
150. M.M. Koton and Yu. N. Sazanov, *Polym.Sci. USSR (Engl. Transl.)*,**15**, 1857 (1973).
151. J.A. Hinkley and B.J. Jensen, *High Perform. Polym.*, **7**, 1 (1995).
152. J.A. Cella, in *Polyimides, Fundamentals and Applications*, M.K. Gosh and K.L. Mittal, eds., Marcel Dekker, New York, 1996, p.343.
153. M.A.B. Meador, J.C. Johnston, P.J. Cavano and A.A. Frimer, *Macromolecules*, **30**, 3215 (1997).
154. A.J. Kinloch, “*Adhesion and Adhesives Science and Technology*”, Chapman and Hall, New York, 1987, p. 196.
155. Annual Book of ASTM Standards, Part 22, American Society for Testing and Materials, Philadelphia, PA, 1982.
156. R. Chait and E.T. Clegg, *Adhesives in Manufacturing*, G.L. Schneberger ed., Marcel Dekker, New York, 1983.
157. A.J. Kinloch, “*Adhesion and Adhesives Science and Technology*,” Chapman and Hall, New York, 1987, p. 311.
158. ASTM Standard D1002-72, Annual Book of ASTM Standards, Adhesives, Vol. 15.06, 1992.
159. R. B. Krieger, Jr., “*Adhesive Bonding Design and Analysis*”, In: Engineered Materials Handbook, Volume 3, Adhesives and Sealants, H.F. Brinson (Ed.), ASM International, Materials Park, Ohio, 1990, p. 472.
160. J.A. Marceau, Y. Moji and J.C. McMillian, *Adhes. Age*, **20**, 28 (1977).

161. ASTM Standard D3762 -79, Annual Book of ASTM Standards, Adhesives, Vol. 15.06, 1984, p. 360.
162. J. Cognard, *J. Adhes.*, **20**, 1 (1986).
163. A.J Kinloch, L.S. Welch, and H. E. Bishop, *J. Adhes.*, **16**, 165 (1984).
164. J. Cognard, *J. Adhes.*, **26**, 155 (1988).
165. M.P. Fuller and P.G. Griffiths, *Anal. Chem.*, **50**, 1906 (1978).
166. M.P. Fuller and P.G. Griffiths, *Appl. Spectrosc.*, **34**, 533 (1980).
167. P. Kubelka, *J. Opt. Soc. Am.*, **38**, 448 (1948).
168. W.W. Wendlandt and H.G. Hecht, “*Reflectance Spectroscopy*”, Interscience, New York (1966).
169. J.R. Reitz, F.J. Minford, and R.W. Christy, “*Foundations of Electromagnetic Theory*”, 3<sup>rd</sup> ed., Addison-Wesley, Reading, Mass. (1979).
170. D. Briggs, “*Practical Surface Analysis by Auger and X-ray Photoelectron Spectroscopy*”, D. Briggs and M.P. Seah, Editors, John Wiley and Sons, Inc., Chichester, 1983.
171. C.D. Wagner, W.M. Riggs, L.E. Davis, and J.F. Moulder, “*Handbook of X-ray Photoelectron Spectroscopy*”, PHI Publication, ed. G.E. Mullenberg, 1979.
172. R.L. Garlach and A.R. Ducharme, *Surf. Sci.*, **32**, 329 (1972).
173. L.A. Harris, *J. Appl. Phys.*, **39**, 1419 (1968).
174. M.P. Seah and W.A. Dench, *Surf. Interface Anal.*, **1**, 4 (1979).
175. A. Joshi, *Crystal Properties and Preparation*, **16**, 95 (1988).
176. J.I. Goldstein, D.E. Newbury, P. Echlin, D.C. Jay, C. Fiori, and E. Lifshin, *Scanning Electron Microscopy and X-Ray Microanalysis – A text for Biologist, Materials Scientists, and Geologists*; Plenum Press: New York, 1981, p. 38.
177. D.E. Newbury and H. Yakowitz, Chapter 6, in “*Practical Scanning Electron Microscopy*”, J.I. Goldstein and H. Yakowitz, ed., Plenum Press, New York, 1975, p. 186.
178. S. Hoffman, *Surf. Interface Anal.*, **9**, 3 (1986).
179. A. Benninghoven, *CRC Crit. Rev. Solid State Sci.*, **June**, 291 (1976).

180. D.E. Newbury, in “*Quantitative Surface Analysis of Materials, ASTM STP 643*”, N.S. McIntyre, ed., American Society for Testing and Materials, 1978, p. 127.
181. A. Brown and J.C. Vickerman, *Surf. Interface Anal.*, **6**, 1 (1984).
182. M. Gettings and A.J. Kinloch, *J. Mat. Sci.*, **12**, 2049 (1977).
183. ASTM Standard D1002 - 94, Annual Book of ASTM Standards, Adhesives, Vol. 15.06, 1994, p. 1.
184. G. Beamson and D. Briggs, “*High Resolution XPS of Organic Polymers - The Scienta ESCA300 Database*”, John Wiley and Sons, New York, p. 214.
185. W.O. Buckley and K. J. Schroeder, “Adhesive Modifiers,” in: *Engineered Materials Handbook, Adhesive and Sealants*, Vol. 3, ASM International, USA, 1990, p. 175.
186. Personal communication, July 20, 1998: Mr. Larry Avery, Technical Support Person, BGF Industries, Inc., Greensboro, NC.
187. H. Ishida and M.T. Huang, *Spectrochimica Acta*, **51**, 319 (1995).
188. H. Ishida, S.T. Wellinghoff, E. Baer and J.L. Koenig, *Macromolecules*, **13**, 826 (1980).
189. J.F. Dezern and P.R. Young, *Int. J. Adhes. and Adhes.*, **5**, 183 (1985).
190. I. Ghosh, J. Konar and A.K. Bhowmick, *J. Adhes. Sci. Technol.*, **11**, 877 (1997).
191. M.F.G. Loustalot and L.D. Cunha, *Polymer*, **39**, 1799 (1998).
192. R.K. Giunta, “*Durability of Polyimide/Titanium Adhesive Bonds: An Interphase Investigation*”, Ph.D. Dissertation, Virginia Polytechnic Institute and State University, Blacksburg, Virginia, October, 1999.
193. W.J. Van Ooij, “*Spectroscopic Techniques in Adhesive Bonding*”, Handbook of Adhesive Technology, eds; A Pizzi and K.L. Mittal, Marcel Dekker, Inc., 1994, p. 192.
194. A. Benninghoven, *Surface Sci.*, **53**, 596 (1975).
195. T.R. Hayes and J.F. Evans, *J. Phys. Chem.*, **88**, 1963 (1984).
196. E. McCafferty, J.P. Wightman, and T. Frank Cromer, *J. Electrochem. Soc.*, **146**, 2849 (1999).
197. E. McCafferty and J.P. Wightman, *Appl. Surf. Sci.*, **143**, 92 (1999).
198. J.S. Solomon and W.L. Baun, *Surf. Sci.*, **51**, 228 (1975).
199. S. Thomas, *Surf. Sci.*, **55**, 756 (1976).

200. M.L. Knotek and J.E. Houston, *Phys. Rev.*, **B15**, 4580 (1977).
201. H.J. Mathieu, J.B. Mathieu, D.E. McClure and D. Landolt, *J. Vac. Sci. Technol.*, **14**, 1023 (1977).
202. C.N.R. Rao and D.D. Sharma, *Phys. Rev.*, **B25**, 2927 (1982).
203. J.T. Grant, T.W. Haas and J.E. Houston, *J. Vac. Sci. Technol.*, **11**, 227 (1974).
204. J. Gandon and J.C. Joud, *J. Less-Common Metals*, **69**, 277 (1980).
205. V.E. Henrich, G. Dresselhaus and H.J. Zieger, *Phys. Rev. Letters*, **36**, 1335 (1976).
206. A.A. Roche, J.S. Solomon and W.L. Baun, *Appl. Surf. Sci.*, **7**, 83 (1981).
207. G.E. McGuire, G.K. Schweitzer, and T.A. Carlson, *Inorg. Chem.*, **12**, 2451 (1973).
208. Y.A. Wang, Y. Miura, and T. Tsugaru, *J. Mater. Sci. Lett.*, **8**, 421 (1989).
209. M. Miyayama, K. Koumoto, and H. Yanagida, "Engineering Properties of single oxides, In: Engineered Materials Handbook, Vol. 4: Ceramics and Glasses; S.J. Schneider, Tech. Chair. (ASM International: USA, 1991), p. 748.
210. Handbook of Chemistry and Physics, D. R. Lide, editor. (CRC Press, Boca Raton, FL, USA), 72<sup>nd</sup> edition, 1991-92, p. 4.

**The vita has been removed from  
the scanned document**